JEM Journal of Experimental Medicine

ARTICLE

EDA fibronectin–TLR4 axis sustains megakaryocyte expansion and inflammation in bone marrow fibrosis

Alessandro Malara[1,2], Cristian Gruppi[1*], Vittorio Abbonante[1,2*], Daniele Cattaneo[3], Luigi De Marco[4,5], Margherita Massa[2], Alessandra Iurlo[3], Umberto Gianelli[6], Carlo L. Balduini[7], Maria E. Tira[8], Andrès F. Muro[9], Anil K. Chauhan[10], Vittorio Rosti[11], Giovanni Barosi[11], and Alessandra Balduini[1,2,12]

The fibronectin EDA isoform (EDA FN) is instrumental in fibrogenesis but, to date, its expression and function in bone marrow (BM) fibrosis have not been explored. We found that mice constitutively expressing the EDA domain (EIIIA$^{+/+}$), but not EDA knockout mice, are more prone to develop BM fibrosis upon treatment with the thrombopoietin (TPO) mimetic romiplostim (TPO^{high}). Mechanistically, EDA FN binds to TLR4 and sustains progenitor cell proliferation and megakaryopoiesis in a TPO-independent fashion, inducing LPS-like responses, such as NF-κB activation and release of profibrotic IL-6. Pharmacological inhibition of TLR4 or TLR4 deletion in TPO^{high} mice abrogated Mk hyperplasia, BM fibrosis, IL-6 release, extramedullary hematopoiesis, and splenomegaly. Finally, developing a novel ELISA assay, we analyzed samples from patients affected by primary myelofibrosis (PMF), a well-known pathological situation caused by altered TPO signaling, and found that the EDA FN is increased in plasma and BM biopsies of PMF patients as compared with healthy controls, correlating with fibrotic phase.

Introduction

Fibronectin (FN) is a glycoprotein of ∼220 kD whose mRNA has three alternative splicing sites (termed extra domain A [EDA], extra domain B [EDB], and IIICS or EIIIA, EIIIB, and V) that allow 20 different isoforms of FN mRNA (White et al., 2008). Circulating plasma FN (pFN) lacks both EDA and EDB segments and is a soluble form secreted by hepatocytes, while cellular FN (cFN) contains variable proportions of EDA and EDB segments and is organized as fibrils in the tissue matrix (Moretti et al., 2007). Extracellular inducers of alternatively spliced FNs are relatively unknown. In this regard, TGF-β1 has been proven to affect the alternative splicing of the EDA exon through the induced expression of the splicing factors SRp40, SRp20, or ASF/SF2 (Borsi et al., 1990; Han et al., 2007). FN containing EDA segment presents unique biochemical properties as compared with the isoform lacking this domain. EDA containing FN has been shown to activate TLR4 in the innate immune response (Okamura et al., 2001). Recently, we demonstrated that mice with constitutive inclusion of EDA exon (EIIIA$^{+/+}$) or knockout for EDA exon (EIIIA$^{-/-}$) display regular hematopoietic homeostasis, although tissue-specific compensations in the amount of FN and in the expression of FN receptors were detected (Malara et al., 2016). Despite this knowledge, to date, expression and function of cFN isoforms in bone marrow (BM) fibrosis have not been explored.

BM fibrosis occurs secondarily to several hematological and nonhematological disorders (Kuter et al., 2007). The pathophysiology underlying BM fibrosis remains unclear despite intensive study, with lack of specific therapy (Kuter et al., 2007). BM fibrosis is characterized by increased numbers of stromal cells, enhanced neoangiogenesis, and hypercellularity in the BM (Cervantes et al., 2009). In addition, patients with BM fibrosis have increased levels of extracellular matrix (ECM) proteins, particularly reticulin, FN fibers, and in some cases, collagen fibers. BM fibrosis is also associated with increased numbers and abnormal functions within the megakaryocyte (Mk) lineage. Aberrant megakaryopoiesis is a hallmark of the myeloproliferative neoplasms (MPNs), a group of clonal hematological

[1]Department of Molecular Medicine, University of Pavia, Pavia, Italy; [2]Laboratory of Biochemistry, Biotechnology and Advanced Diagnostics, Istituto di Ricovero e Cura a Carattere Scientific San Matteo Foundation, Pavia, Italy; [3]Hematology Division, Istituto di Ricovero e Cura a Carattere Scientific Ca' Granda-Maggiore Policlinico Hospital Foundation, Milan, Italy; [4]Department of Translational Research, National Cancer Center (Istituto di Ricovero e Cura a Carattere Scientific Centro di Riferimento Oncologico), Aviano, Italy; [5]Department of Molecular and Experimental Research, The Scripps Research Institute, La Jolla, CA; [6]Division of Pathology, Department of Pathophysiology and Transplantation, University of Milan, Milan, Italy; [7]Department of Internal Medicine, Istituto di Ricovero e Cura a Carattere Scientific San Matteo Foundation, Pavia, Italy; [8]Department of Biology and Biotechnology "Lazzaro Spallanzani," University of Pavia, Pavia, Italy; [9]The International Center for Genetic Engineering and Biotechnology, Trieste, Italy; [10]Department of Internal Medicine, University of Iowa, Iowa City, IA; [11]Center for the Study of Myelofibrosis, Laboratory of Biochemistry, Biotechnology and Advanced Diagnostics, Istituto di Ricovero e Cura a Carattere Scientific Policlinico S. Matteo Foundation, Pavia, Italy; [12]Department of Biomedical Engineering, Tufts University, Medford, MA.

*C. Gruppi and V. Abbonante contributed equally to this paper; Correspondence to Alessandra Balduini: alessandra.balduini@tufts.edu.

malignancies originating from hematopoietic stem cells (HSCs), leading to an increase in mature blood cells in the peripheral blood (Tefferi et al., 2007). MPNs have been classified by the World Health Organization (WHO) as a single group; however, they comprise three clinically defined disorders caused by altered JAK/STAT signaling, called polycythemia vera (PV), essential thrombocythemia (ET), and primary myelofibrosis (PMF; Vannucchi et al., 2009; Vardiman et al., 2009). Three MPN-restricted driver mutations have been described so far, including those in JAK2, calreticulin, and myeloproliferative leukemia virus (James et al., 2005; Pardanani et al., 2006; Klampfl et al., 2013; Nangalia et al., 2013). Among MPNs, PMF is a pathological condition characterized by a profound alteration of BM structure and matrix composition. Patients affected by this pathology display a high number of atypical Mk's within the BM and progressive accumulation of reticulin and collagen, which compromises patient prognosis (Kuter et al., 2007). Mk's are presumed to be the neoplastic cell subtype that predominantly forces fibroblasts to produce ECMs in the disease, through an uncontrolled production and release of several cytokines, such as transforming growth factor-β1 (TGF-β1), platelet-derived growth factor, or basic fibroblast growth factor (Malara et al., 2015). More than three decades ago, decreased plasma levels of FN were reported in PMF patients, while an abnormal form of FN, designated as FN-C, was found in seven plasma samples of PMF patients by immunoassays (Norfolk et al., 1983; Vellenga et al., 1985). More recently, FN has been implicated in the aberrant interactions between the stromal and hematopoietic compartments within the BM niche of PMF patients, as increased FN synthesis was detected in both BM-derived mesenchymal stem cells (MSCs) of prefibrotic and overt fibrotic PMF patients as well as in osteoblasts derived from PMF patients (Schneider et al., 2014; Abbonante et al., 2016b; Avanzini et al., 2018). On the contrary, expression and function of cFN isoforms in PMF patients have not been explored to date.

On this premise, in this study, we evaluated the potential impact of alternatively spliced EDA FN during BM fibrosis development and progression.

Results

Expression of EDA FN during BM fibrosis in vivo

To analyze the potential role of EDA FN in promoting BM fibrosis, we used a thrombopoietin (TPO)^{high} murine model (Kuter et al., 2009; Léon et al., 2012) based on repeated intracutaneous injections of supra-pharmacological doses of romiplostim every 3 d for 30 d (Fig. 1 A). This model is known to recreate the phenotype of BM fibrosis, shared by patients, together with several hematological features of the disease such as an increased BM Mk number, peripheral thrombocytosis, elevated BM TGF-β1 levels, reticulin and collagen deposition, and splenomegaly because of the increase of extramedullary hematopoiesis (Villeval et al., 1997; Yanagida et al., 1997). FN splicing at EDA, EDB, and V region sites was evaluated by PCR splicing assay in BM cells from saline-treated or TPO^{high} mice during fibrosis progression (Fig. 1 B). Our results confirmed that induction of fibrosis resulted in a significant increase in the rate of EDA inclusion in the BM environment but not of EDB domain (Fig. 1, C and D). In addition, we detected variation in the splicing pattern of V region (Fig. 1 C). Consistently, higher amounts of EDA FN were detected by Western blotting in cell-free BM fluids of TPO^{high} mice with respect to saline-treated mice (Fig. 1, E and F). We also performed a detailed analysis of EDA FN mRNA expression in several BM lineages after the establishment of experimental fibrosis. A prominent up-regulation in EDA FN expression was revealed in the endothelial CD45$^-$Ter119$^-$CD31$^+$ and stromal CD45$^-$Ter119$^-$CD31$^-$PDGFRα$^+$ cell populations after fibrosis development (Fig. 1 G). The CD45$^+$Ter119$^-$ hematopoietic fraction and CD45$^+$/CD41$^+$ Mk's did not exhibit significant up-regulation of EDA FN (Fig. 1 G). Moreover, several FN receptors were up-regulated in BM cells after experimental fibrosis. Interestingly, among different TLRs, expression of TLR4 was strongly increased (Fig. 1 H).

Mice with forced inclusion of EDA exon of FN are more prone to experimental BM fibrosis in vivo

To investigate the role of EDA FN on fibrosis in vivo, we exploited two unique transgenic mouse models unable to undergo alternative splicing of the EDA FN exon. One strain contains optimized spliced sites at both splicing junctions of the EDA exon and constitutively includes the exon (EIIIA$^{+/+}$), whereas the other strain contains an EDA-null allele of the EDA exon (EIIIA$^{-/-}$; Muro et al., 2003; Fig. 2 A).

Induction of BM fibrosis with the TPO^{high} model demonstrated that EIIIA$^{+/+}$ mice were more prone to develop Mk hyperplasia and myelofibrosis with respect to EIIIA$^{-/-}$ mice. Flow cytometry analysis of BM from these mice revealed that the frequency of HSC-enriched LSK (Lin$^-$Sca1$^+$c-kit$^+$) cells and short-term HSCs (ST-HSCs) was significantly increased in the EIIIA$^{+/+}$ mice with respect to wild-type and EIIIA$^{-/-}$ mice (Fig. 2 B and Fig. S1 A). Spleens of wild-type and EIIIA$^{+/+}$ mice also exhibited increased percentages of multipotent progenitors (MMPs) and myeloid progenitors (LKs), in particular of common myeloid progenitors (CMPs) and Mk/erythroid progenitors (MEPs) compared with EIIIA$^{-/-}$ mice (Fig. 2 C and Fig. S1 B). Differently from wild-type and EIIIA$^{+/+}$ mice, deletion of EIIIA exon restrained the loss of medullary erythropoiesis and the appearance of CD71^{high}Ter119^{high} (stage II) erythroid precursors in the spleen (Fig. S1, C–F). Progenitor colony assay showed increased CFU-GM colonies in the BM and spleens of EIIIA$^{+/+}$ mice but comparable burst-forming units–erythroid (BFU-E; Fig. S1, G and H). In contrast, the frequency of Mk's was significantly increased in the BM and spleens of wild-type and EIIIA$^{+/+}$ mice compared with EIIIA$^{-/-}$ mice (Fig. 2, D–J). These results suggest that inclusion of EDA domain of FN sustains TPO-dependent LSK expansion and megakaryopoiesis in mice.

Additionally, mice with constitutive inclusion of EDA exons displayed increased susceptibility to BM fibrosis progression as revealed by the amount of reticulin fibers deposition at the end of experimental BM fibrosis (Fig. 2, K and L). Further, EIIIA$^{-/-}$ mice presented normal spleen size and weight and very little extramedullary hematopoiesis (Fig. 2, M and N). Finally, EIIIA$^{+/+}$ mice exhibited marked peripheral blood thrombocytosis after experimental fibrosis (Fig. 2 O),

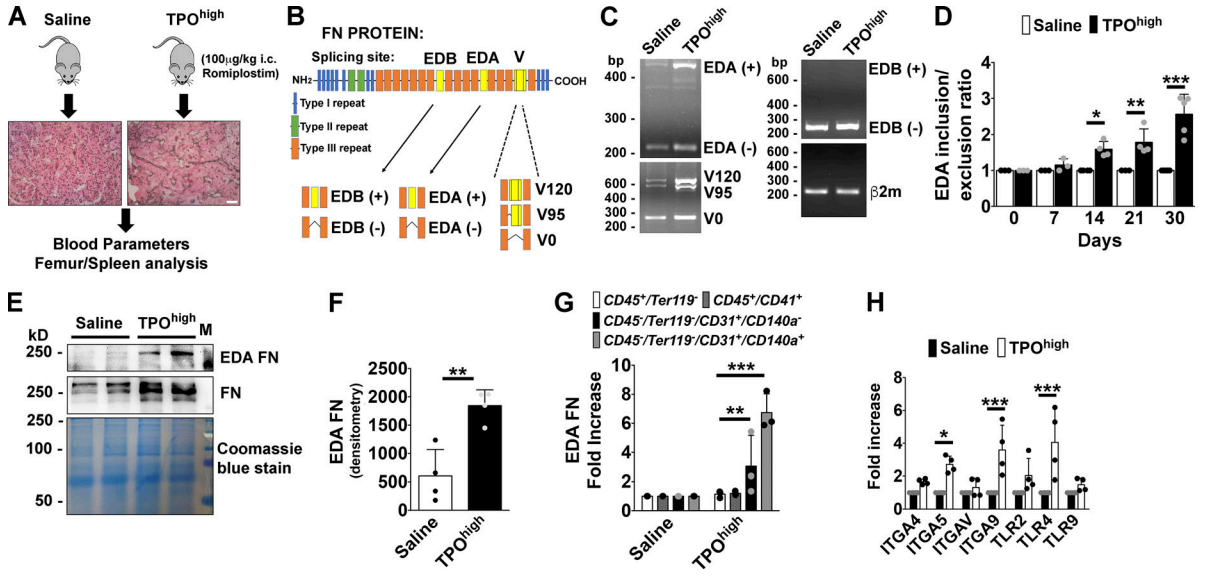

Figure 1. **Expression of EDA FN during BM fibrosis progression. (A)** A TPO^{high} mouse model was established to induced BM fibrosis in wild-type (wt/wt) mice. Mice received subcutaneous injections of either vehicle (saline, PBS) or romiplostim (100 µg/kg of body weight) every 3 d for 1 mo. Bar, 50 µm. **(B)** Scheme of alternative splicing sites in full-length FN subunit protein. **(C)** Splicing of alternative exon EDA, EDB exon, and V region of FN were analyzed by PCR assay in BM cells from saline-treated or TPO^{high} mice. (+) mRNA indicates inclusion and (–) mRNA indicates exclusion of the EDA or EDB exon. Splicing of the V0, V120, and V95 variants of the V region are also indicated. β2m was used for comparative concentration analysis. **(D)** Densitometry analysis of the ratio between FN mRNA including and excluding EDA exon. Ratios were determined relative to saline treated mice (1.0) at days 0, 7, 14, 21, and 30 of TPO treatment. n = 4. **(E)** Cell-free fluids from femurs of saline or TPO^{high} mice were analyzed for FN content in Western blotting. EDA FN was revealed with the antibody FN3E2 specific for EDA domain. Membrane was then reprobed with a polyclonal antibody to total FN. Coomassie blue staining was performed for comparative concentration analysis. **(F)** Densitometry analysis of EDA FN protein in cell-free BM fluids. Results were determined relative to saline-treated mice (1.0). n = 4. **(G)** Real-time PCR of EDA FN expression in sorted hematopoietic CD45$^+$/Ter119$^-$ cells, CD45$^+$/CD41$^+$ Mk's, CD45$^-$/Ter119$^-$CD31$^+$ endothelial cells, and CD45$^-$/Ter119$^-$/CD31$^-$/CD140a$^+$ stromal cells from saline-treated or TPO^{high} mice. n = 3. **(H)** Real-time PCR analysis of integrins and TLRs expression in BM cells from saline-treated or TPO^{high} mice. n = 4. *, P < 0.05; **, P < 0.01; ***, P < 0.001. i.c., intracutaneous. Data are shown as mean ± SD.

while white and red blood cell counts were not statistically different (Fig. 2, P and Q).

EDA FN synergizes with TPO in sustaining Mk proliferation through the activation of common STAT-5 and ERK 1/2 signaling pathways

To investigate the molecular role of EDA FN during BM fibrosis progression, we analyzed the effects of the different FN isoforms on BM hematopoietic progenitors and Mk's, which are presumed to play a pivotal role in the pathogenesis of the disease (Ciurea et al., 2007). In the first approach, we tested whether the EDA segment was capable of increasing the proliferation or survival of BM hematopoietic progenitor cells. Lineage negative (Lin$^-$) cells from wild-type mice were purified and seeded at 2 × 10^5/ml for 4 d in standard medium supplemented only with 1 µg of recombinant peptides containing (EDA$^+$) or not containing (EDA$^-$) the EDA domain. In addition, cells were also stimulated with recombinant mouse TPO (10 ng/ml) alone or in combination with the EDA$^+$ peptide to verify their synergy observed in vivo in the EIIIA$^{+/+}$ mice. Prior to use, peptides were analyzed with a monoclonal antibody targeting the EDA domain of FN, or a polyclonal antibody that recognizes both FN containing or lacking the EDA segment (Fig. 3 A).

Absolute cell numbers at the end of cultures were statistically different in TPO-treated cells, while a significant increase in cell survival was detected at the end of culture in cells stimulated with EDA$^+$ peptide, TPO, and their combination (Fig. 3, B and C). However, differently from EDA$^-$ peptide, cell stimulation with EDA$^+$ peptide increased the frequency and the percentage of BrdU-incorporating LSK cells after 24 h, without affecting their survival (Fig. 3, D–F). Interestingly, EDA$^+$ peptide seemed to synergize with TPO in this function (Fig. 3, E and F). Consistently, analysis of CD41$^+$ Mk output by flow cytometry at different days of culture demonstrated that only the EDA$^+$ peptide was able to sustain Mk differentiation in a TPO-independent manner. Synergism between EDA$^+$ peptide and TPO was further confirmed in sustaining Mk differentiation (Fig. 3 G). To explain these results, we reasoned that addition of the EDA FN to the culture medium should activate signaling pathways related to Mk differentiation. Thus, to ascertain that this effect was peculiar of the EDA domain and maintained within the structure of native protein, we tested the ability of full-length proteins containing or not the EDA domain to activate signaling pathways underlying Mk maturation, in the absence of TPO. Therefore, fetal liver–differentiated Mk's were serum-starved and then stimulated for 30 and 60 min with 5 µg of human pFN (lacking the EDA domain), or cFN derived from human skin fibroblasts (containing the EDA domain). Western blot analysis revealed increased STAT-5 and ERK 1/2 phosphorylation in Mk's stimulated with cFN with respect to untreated cells or cells stimulated with pFN (Fig. 3, H and I). Increased STAT-5 phosphorylation upon cFN stimulation, with respect to pFN, was further

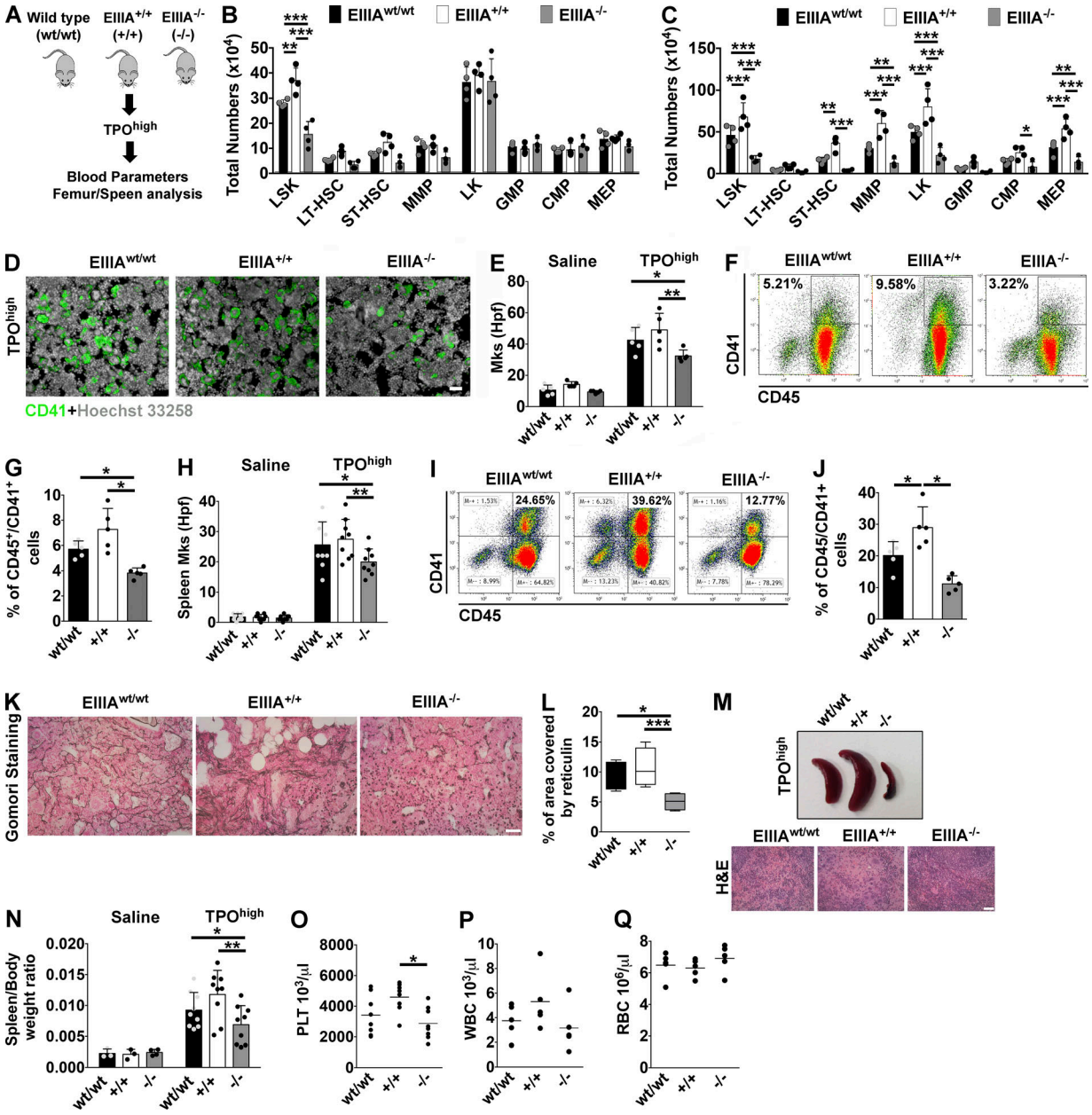

Figure 2. **Mice with forced inclusion/exclusion of EDA exon showed different degrees of susceptibility to experimental BM fibrosis. (A)** Schematic representation of strategy used to induce BM fibrosis in EIIIA$^{wt/wt}$, EIIIA$^{+/+}$, and EIIIA$^{-/-}$ mice. **(B and C)** Total numbers of LSK, long-term HSC (LT-HSC), ST-HSC, MMP, CMP, GM progenitor (GMP), and MEP cells in the BM (B) and spleens (C) of mice treated with TPO (n = 4). **(D)** Representative CD41 staining on BM sections of TPO^{high}-treated mice. Bar, 50 µm. Objective, 20×. **(E)** Quantification of Mk numbers per high power field (hpf) in saline- (n = 6) and TPO^{high}-treated mice (n = 5). **(F)** Representative dot plots of flow cytometric analysis of CD45/CD41^{+} Mk's in the BM of EIIIA$^{wt/wt}$, EIIIA$^{+/+}$, and EIIIA$^{-/-}$ mice treated with TPO. **(G)** Frequencies of BM CD45/CD41^{+} Mk's in TPO-treated mice (n = 5). **(H)** Quantification of Mk number per hpf in spleen sections of TPO-treated mice. Mk's were counted from at least nine random images of spleen sections per mice, with three mice per genotype. **(I and J)** Representative dot plots of flow cytometric analysis of Mk's in the spleen of EIIIA$^{wt/wt}$, EIIIA$^{+/+}$, and EIIIA$^{-/-}$ mice treated with TPO (I) and relative frequency quantification (J; n = 5). **(K)** Representative Gomori staining of BM sections from TPO-treated mice. Bar, 50 µm. Objective, 20×. **(L)** Assessment of reticulin deposition in EIIIA$^{wt/wt}$, EIIIA$^{+/+}$, and EIIIA$^{-/-}$ mice in the TPO^{high} model. **(M)** Representative spleens and H&E staining of spleen sections from EIIIA$^{wt/wt}$, EIIIA$^{+/+}$, and EIIIA$^{-/-}$ mice in the TPO^{high} model. Bar, 50 µm. **(N)** Spleen-weight to body-weight ratios in saline- (n = 3) and TPO^{high}-treated mice (n = 9). **(O–Q)** Peripheral platelet (PLT; O; n = 8), white (WBC; P), and red blood cell (RBC; Q; n = 5) counts in TPO^{high}-treated mice. *, P < 0.05; **, P < 0.01; ***, P < 0.001. Data are shown as mean ± SD.

confirmed by immunoprecipitation assay (Fig. 3 J). Interestingly, effects of cFN on Mk signaling were concentration dependent (Fig. S1, I–K). To confirm that EDA FN and TPO act through common signaling pathways, we measured the phosphorylation levels of STAT-5 and ERK 1/2 kinases in Lin^{-} cell cultures stimulated for 4 d with TPO and recombinant peptides (Fig. 3, K and L). Increased levels of STAT-5 and ERK 1/2 activation were detected by Western blotting in cells supplemented with TPO

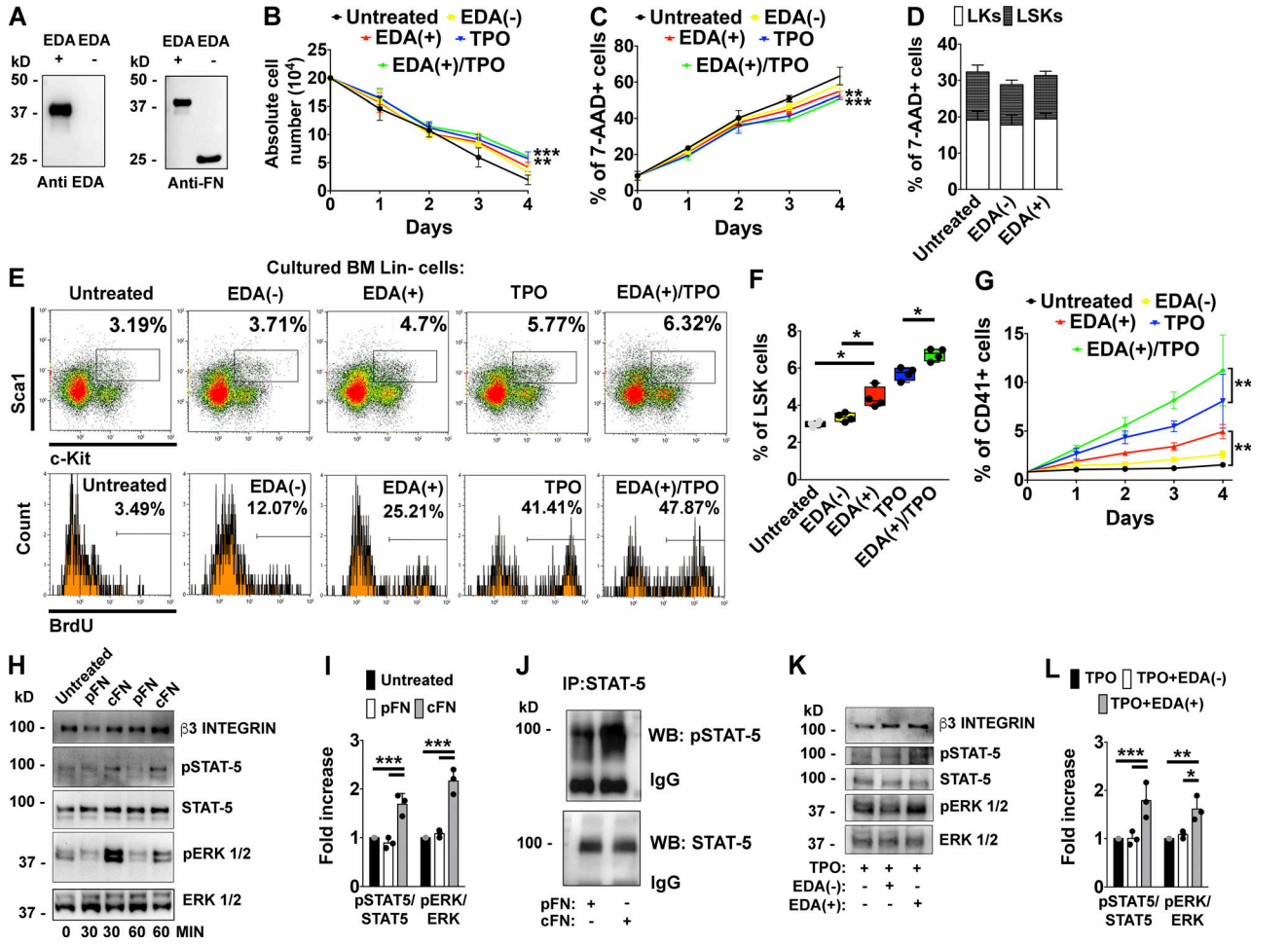

Figure 3. **EDA domain of FN sustains hemopoietic progenitor cells proliferation and Mk development in vitro. (A)** 1 µg of recombinant peptides containing (EDA^+) or lacking EDA (EDA^-) segment of FN were tested by Western blot with a monoclonal anti-EDA segment or a polyclonal rabbit anti-FN. **(B)** Lin^- fractions from BM cells were maintained in DMEM for 4 d in the presence of 1 µg of EDA^+ and EDA^- recombinant peptides, 10 ng/ml of TPO, and TPO plus EDA^+ peptide. Absolute cell numbers at different days are shown. $n = 3$. **(C)** Assessment of cell mortality by flow cytometry in the different experimental conditions using 7-AAD staining. $n = 3$. **(D)** Effects of EDA^+ and EDA^- peptides on LSKs and LKs survival after 24 h of culture were tested by 7-AAD staining. $n = 3$. **(E)** Upper panels: Representative flow cytometry analysis of LSK frequencies in vitro after stimulation with recombinant peptides, TPO, or TPO plus EDA^+ peptide for 24 h. Lower panels: Percentage of $BrdU^+$ proliferating cells in the LSKs gate. **(F)** Frequencies of LSK cells in Lin^- cells stimulated with recombinant peptides, TPO, or TPO plus EDA^+ peptide for 24 h. $n = 4$. **(G)** Quantification of $CD41^+$ Mk's at different days of culture was evaluated by flow cytometry analysis. $n = 3$. **(H)** Fetal liver–derived Mk's were stimulated for 30 or 60 min, with 5 µg of pFN or cFN, or left untreated. STAT-5 and ERK 1/2 phosphorylation was then evaluated by Western blot. β3 integrin was revealed to ensure the same number of Mk's used in the experiment. **(I)** Histograms showing the ratio of phosphorylated and total STAT-5 and ERK 1/2 proteins in Mk's stimulated with pFN or cFN for 1 h. $n = 3$. **(J)** Mk's were stimulated with pFN or cFN for 1 h. STAT-5 was immunoprecipitated (IP) from cell lysates and tested with a phospho–STAT-5 antibody (pSTAT-5). IgG indicates IgG chains. WB, Western blot. **(K)** Representative Western blot analysis of STAT-5 and ERK 1/2 phosphorylation in BM Lin^- cells differentiated with TPO alone or TPO plus 1 µg of EDA^- or EDA^+ peptides for 4 d. **(L)** Histograms showing the ratio of phosphorylated and total STAT-5 and ERK 1/2 proteins in BM Lin^- cells differentiated with TPO alone or TPO plus EDA^- or EDA^+ peptides for 4 d. $n = 3$. *, $P < 0.05$; **, $P < 0.01$; ***, $P < 0.001$. Data are shown as mean ± SD.

plus the EDA^+ peptide with respect to cells treated with TPO only or TPO plus the EDA^- peptide.

Effects of EDA FN on Mk's are dependent on TLR4 engagement

Inclusion of the EDA segment in the FN protein introduces new binding sites for integrins, such as α4β1, α4β7, and α9β1 (Liao et al., 2002; Shinde et al., 2008; Kohan et al., 2010). Moreover, EDA domain has been demonstrated to activate the nonintegrin receptor, TLR4, involved in the innate immune response. Thus, we aimed at identifying the receptor that was responsible for mediating the EDA FN–dependent effects on Mk function. Fetal liver–derived Mk's were stimulated for 1 h with 1 µg of purified cFN or left untreated. Cells were then lysed and the extracted proteins split into two pools from which TLR4 and α4 integrin subunit were immunoprecipitated separately. Co-immunoprecipitation of cFN with both receptors was then analyzed by means of a specific anti-EDA antibody. As shown in Fig. 4 A, a significant engagement of TLR4, and to a lesser extent α4 integrin, was evident in Mk's stimulated with cFN but not in untreated cells, suggesting that EDA FN/TLR4 interaction is the prominent event underlying Mk–EDA FN recognition. To confirm the pivotal role of TLR4 in mediating the EDA FN effects, we

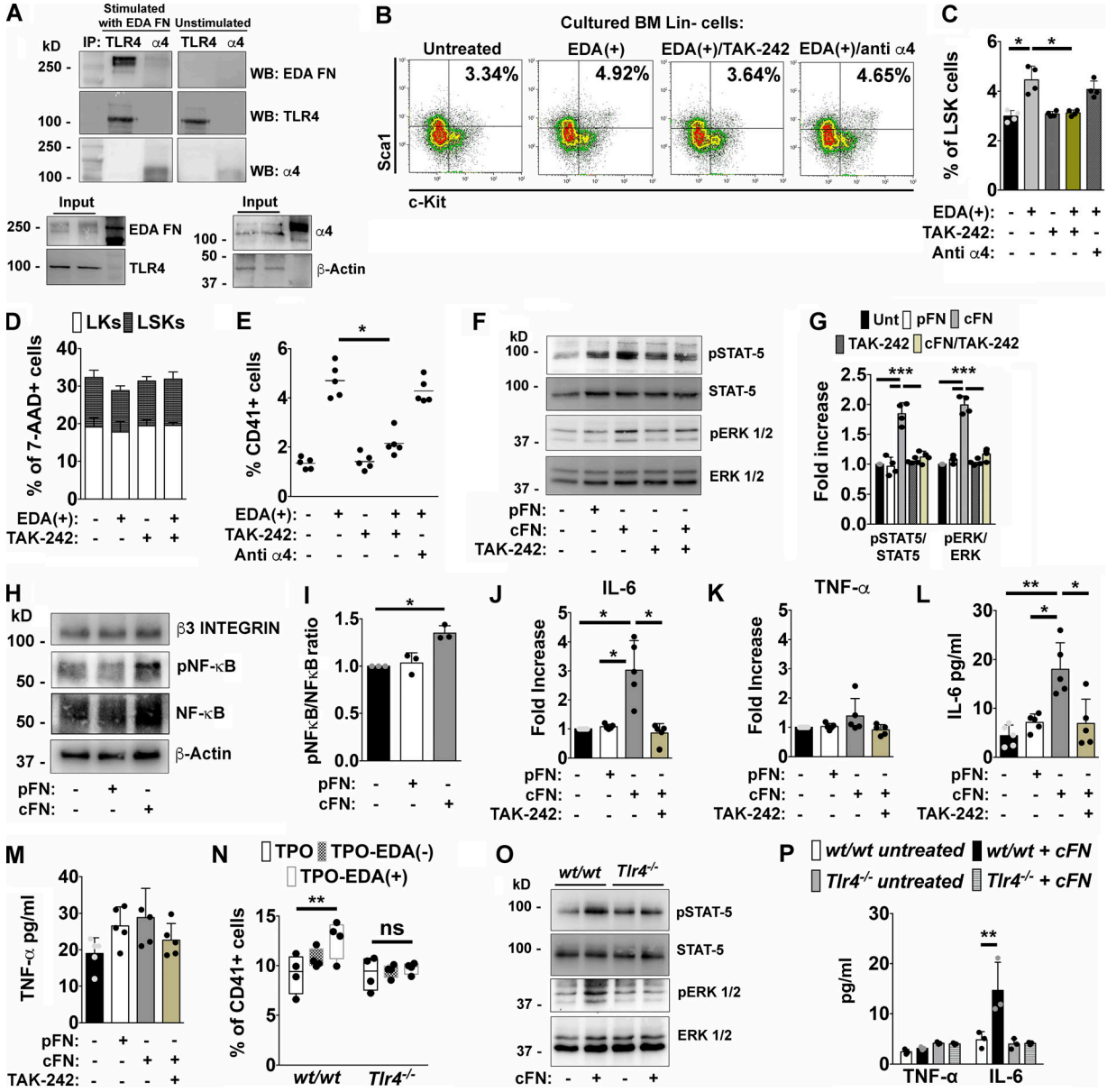

Figure 4. **Effects of EDA domain on Mk's are TLR4 dependent. (A)** Purified Mk's were incubated for 1 h with 1 µg of cFN or left untreated, centrifuged, and lysed. Extracted proteins from both samples were split and TLR4 and α4 integrin immunoprecipitated (IP) from the two fractions of proteins, respectively. Co-immunoprecipitated cFN was then revealed in both fractions by Western blot (WB). Inputs: proteins in total cell lysates. Actin was detected from the cell lysate to ensure equal protein loading. **(B and C)** Representative dot plots of LSKs in Lin⁻ cells cultured for 24 h with 1 µg of EDA⁺ peptide, or pretreated with TAK-242 (1 µg/ml) or an anti–α4 integrin antibody with blocking function (10 µg/ml) before EDA⁺ stimulation (B) and relative quantification (C). *n* = 4. **(D)** Flow cytometry analysis of 7-AAD⁺ dead LK and LSK cells after 24 h of culture with TAK-242 alone or in combination with EDA⁺ peptide. *n* = 3. **(E)** Quantification of CD41⁺ Mk's derived from Lin⁻ cells left unstimulated or stimulated with 1 µg of EDA⁺ peptide or pretreated with TAK-242 or an anti–α4 integrin antibody for 4 d. *n* = 5. **(F)** Purified Mk's were left untreated or stimulated for 1 h with 5 µg of pFN, cFN, and TAK-242 alone and before cFN stimulation. STAT-5 and ERK 1/2 phosphorylation were then evaluated by Western blotting. **(G)** Histograms showing the ratio of phosphorylated and total STAT-5 and ERK 1/2 proteins in mature Mk's unstimulated or stimulated with pFN, cFN, and TAK-242 alone and before cFN stimulation. *n* = 3. **(H)** Level of NF-κB activation in Mk's stimulated with cFN for 1 h. β3 was revealed to ensure the same Mk number for each experimental condition. β-Actin was used as equal loading control. **(I)** Histograms showing the ratio of phosphorylated and total NF-κB in Mk's left unstimulated or stimulated with 5 µg of pFN or cFN. *n* = 3. **(J and K)** Fold increase in IL-6 (J) and TNF-α (K) mRNA expression in Mk's after 24 h of co-culture with pFN, cFN, and TAK-242 before cFN addition. *n* = 5. **(L and M)** IL-6 (L) and TNF-α (M) quantification by ELISA in culture supernatants from untreated and treated Mk's. *n* = 5. **(N)** Quantification of CD41⁺ Mk's derived from *wt/wt* and *Tlr4*$^{-/-}$ BM Lin⁻ cells differentiated with TPO, TPO plus EDA⁺ peptide, or EDA⁻ peptide. *n* = 4. **(O)** Western blot analysis of STAT-5 and ERK 1/2 activation in *wt/wt* and *Tlr4*$^{-/-}$ Mk's, left untreated or stimulated with 5 µg of cFN for 1 h. *n* = 2. **(P)** TNF-α and IL-6 quantification in culture supernatants from wt/wt and *Tlr4*$^{-/-}$ Mk's untreated, or treated with cFN. *n* = 3. *, P < 0.05; **, P < 0.01; ***, P < 0.001; ns, not significant. Data are shown as mean ± SD.

pretreated BM Lin⁻ cells with a pharmacological inhibitor of TLR4 (TAK-242; 1 µg/ml), or with an α4 antibody with blocking function (10 µg/ml), and assessed LSK cells proliferation and Mk output. As shown in Fig. 4 (B and C), TAK-242, but not α4 antibody, abrogated the proliferative effect of EDA⁺ peptide on LSK cells without affecting their survival (Fig. 4 D). Similarly, inhibition of TLR4 with TAK-242, despite the concomitant stimulation with the EDA segment, resulted in a significant reduction of Mk differentiation to a level comparable to untreated cells. On the contrary, inhibition of α4 integrin had no consequences on EDA-dependent effects on Mk output (Fig. 4 E).

Further, activation of signaling pathways involving STAT-5 and ERK 1/2 was strongly reduced in Mk's pretreated with TLR4 inhibitor, before stimulation with 5 µg of cFN for 1 h (Fig. 4, F and G).

Moreover, Mk's express several members of the TLR family, such as TLR2 and TLR9, that are known to share common signaling pathways with TLR4. To exclude the potential contribution of other TLRs in these processes, we tested their activation during Mk differentiation. Treatment of BM Lin⁻ cells with peculiar agonists of TLR2 and TLR9, Pam(3)CySK(4) and CpG oligodeoxynucleotide (ODN), respectively, did not recapitulate the effects of EDA FN on Mk output. Consistently, LPS, the natural exogenous ligand of TLR4, was able to induce Mk proliferation to a comparable extent as EDA FN (Fig. S1 L).

EDA FN sustains in vitro differentiation of Mk's with a profibrotic phenotype

It is well established that stimulation of TLR4 by LPS induces the release of critical proinflammatory cytokines, through NF-κB activation, that are necessary to activate potent immune responses (Chow et al., 1999). Thus, based on the ability of EDA FN to induce LPS-like responses, we evaluated its potential role in conferring a proinflammatory phenotype to Mk's. Fetal liver–derived Mk's were stimulated for 1 h with 5 µg of cFN or pFN, and the phosphorylation level of NF-κB was analyzed by Western blot. As shown in Fig. 4 (H and I), only the cFN induced a significant activation of this signaling pathway. Consequently, treatment of Mk's with cFN for 24 h, but not with pFN, resulted in increased expression of IL-6 mRNA and protein release in culture supernatants (Fig. 4, J and L), while effects on TNF-α synthesis and release were not significantly different (Fig. 4, K and M). Importantly, inhibition of TLR4 with TAK-242 resulted in a significant reduction of cytokine synthesis and secretion (Fig. 4, J and L). Finally, BM Lin⁻ cells isolated from *Tlr4*$^{-/-}$ mice were unresponsive to EDA FN in terms of Mk differentiation (Fig. 4 N), while cFN-dependent activation of STAT-5 and ERK 1/2 signaling pathways was abolished in Mk's derived from *Tlr4*$^{-/-}$ mice but not from *wt/wt* mice (Fig. 4 O). Consistently, IL-6 release was abrogated in Mk's with TLR4 deletion despite cFN stimulation, while TNF-α levels did not change (Fig. 4 P).

TLR4 is involved in Mk proliferation that characterizes fibrosis development in vivo

To explore the potential role of TLR4 in hematopoietic progenitor cell proliferation and Mk differentiation, *wt/wt* TPO^{high} mice model was treated with daily injections of TAK-242 (1 mg/kg of mice) or vehicle (DMSO 5% vol/vol; Fig. 5 A). Inhibition of TLR4 resulted in reduced BM and spleen content of LSKs, ST-HSCs, MMPs, and MEPs (Fig. 5, B and C; and Fig. S2 A). Medullary erythropoiesis was partially restored after TLR4 inhibition in mice (Fig. S2, B and C) with a concomitant reduction of erythroid progenitors in the spleen (Fig. S2, D and E). Hematopoietic progenitor colonies were reduced in BM and spleens of TAK-242–treated mice with respect to TPO^{high} mice (Fig. S2, F and G).

Immunofluorescence and flow cytometry analysis of BM and spleens of TPO^{high} mice treated with TAK-242 showed a marked decrease in the frequency of CD41⁺ Mk's with respect to TPO^{high} mice treated with vehicle (Fig. 5, D–H). Quantification of BM reticulin fibers after Gomori staining showed a significant reduction in BM fibrosis in mice treated with TAK-242 with respect to vehicle (Fig. 5, I and J). In accordance with these results, mice treated with TAK-242 displayed lower levels of FN and type III collagen deposition in BM sections at the end of treatment (Fig. 5, K–M).

Uncontrolled release of proinflammatory cytokines by proliferating Mk's is a hallmark of BM fibrosis in MPN patients (Tefferi et al., 2011). Interestingly, Mk expansion in the TPO^{high} model was accompanied by a significant rise in IL-6 levels, while TNF-α levels, differently from human patients, were not significantly affected. These cytokines were differently released also in mice with aberrant EDA exon splicing during fibrosis progression, with the EIIIA$^{+/+}$ mice presenting higher levels of BM IL-6 with respect to EIIIA$^{-/-}$ mice (Fig. S2, H and I).

As demonstrated in vitro, TLR4 inhibition in vivo was capable of restraining IL-6 production within BM, while TNF-α levels were unaffected (Fig. 5, N and O). Similarly, increase in spleen size and extramedullary hematopoiesis (Fig. 5, P and Q) were counteracted by TAK-242 treatment. On the other hand, reactive peripheral thrombocytosis, leukocytosis, and anemia were mildly attenuated by TAK-242 treatment, although the differences were not statistically different (Fig. 5, R–T).

Consistently, pharmacological inhibition of TLR4 in mice with altered EDA exon splicing (Fig. S3 A) significantly abrogated Mk hyperplasia (Fig. S3, B and C) and reticulin deposition (Fig. S3, D and E) in EIIIA$^{+/+}$ mice, while it had negligible effects on mice lacking EDA exon of FN. We next verified whether TAK-242 therapy could decrease fibrosis after its formation. BM fibrosis was established in wild-type TPO^{high} mice. Mice were then treated for an additional 2 wk with TPO plus vehicle or TPO plus TAK-242 (Fig. S3 F). As shown in Fig. S3 (G and H), delayed TAK-242 treatment was less effective on BM reticulin deposition, but improved splenomegaly (Fig. S3, I and J).

TLR4 knockout mice are protected from BM fibrosis in vivo

To definitively prove the role of TLR4 in promoting BM fibrosis, *Tlr4*$^{-/-}$ mice were challenged with the TPO^{high} model (Fig. 6 A). BM cells of untreated mice showed regular expression of EDA FN, FN, and other TLRs (TLR2 and TLR9) with respect to *wt/wt* mice (Fig. S4, A and B). In addition, *Tlr4*$^{-/-}$ mice showed a slight reduction in BM Mk content and mild thrombocytopenia (Fig. S4, C–E). Analysis of BM and spleens after experimental fibrosis revealed that hematopoietic progenitor cell proliferation and Mk

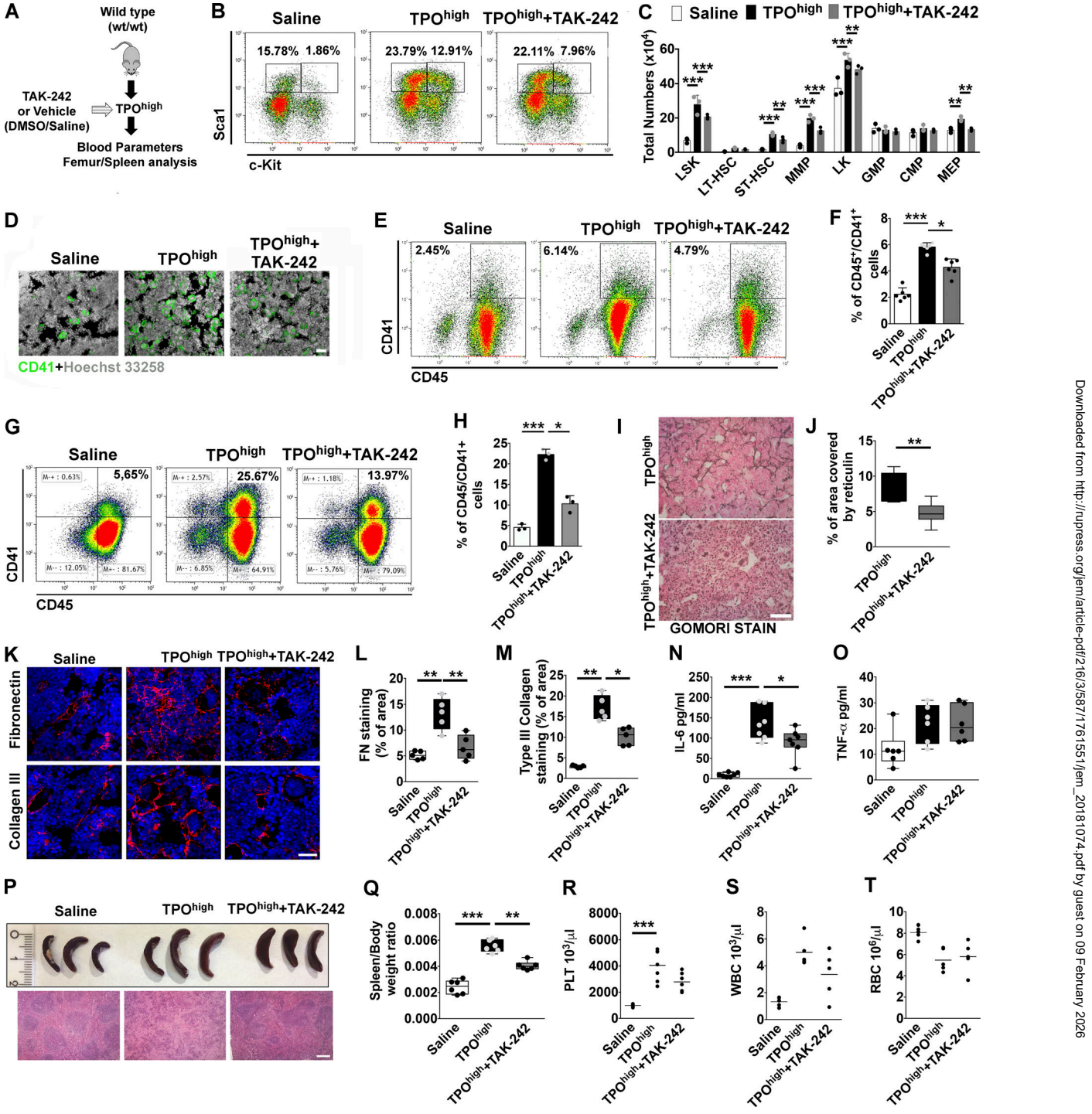

Figure 5. **Pharmacological inhibition of TLR4 in vivo restrains Mk hyperplasia and fibrosis. (A)** Schematic representation of in vivo strategy for TLR4 inhibition in the TPO^{high} mouse model. wt/wt mice undergoing repeated romiplostim injection were concomitantly treated with daily injections of TAK-242 (TPO^{high} plus TAK-242) or vehicle (DMSO in saline; TPO^{high}). **(B)** Representative dot plots of LSKs frequencies in BM of saline-, TPO^{high} plus vehicle–, and TPO^{high} plus TAK-242–treated mice. **(C)** Total numbers of LSK, LT-HSC, ST-HSC, MMP, CMP, GMP, and MEP cells in the BM of saline-, TPO^{high} plus vehicle–, and TPO^{high} plus TAK-242–treated mice are shown in bar graphs as mean ± SD. n = 3. **(D)** Immunofluorescence of BM CD41$^+$ Mk's in saline-, TPO^{high} plus vehicle–, and TPO^{high} plus TAK-242–treated mice. Bar, 50 µm. Objective, 20×. **(E and F)** Representative flow cytometry analysis of CD45/41$^+$ Mk's (E) and relative quantification (F) in BM cells of saline-, TPO^{high} plus vehicle–, and TPO^{high} plus TAK-242–treated mice. n = 6. **(G and H)** Flow cytometry analysis of CD45/41$^+$ Mk's (G) and relative quantification (H) in spleen cells of saline-, TPO^{high} plus vehicle–, and TPO^{high} plus TAK-242–treated mice. n = 6. **(I)** Gomori staining of BM sections from TPO^{high} plus vehicle– and TPO^{high} plus TAK-242–treated mice. Bar, 50 µm. Objective, 20×. **(J)** Quantitative assessment of reticulin deposition in BM sections of mice. **(K)** Immunofluorescence staining of FN and type III collagen in BM sections of saline-, TPO^{high} plus vehicle–, and TPO^{high} plus TAK-242–treated mice. Bar, 50 µm. Objective, 60×. **(L and M)** Quantitative assessment of FN (L) and type III collagen (M) staining was performed in at least 10 random images from BM diaphysis per mice, with five mice per treatment. **(N and O)** Levels of IL-6 (N; n = 7) and TNF-α (O; n = 6) were measured by ELISA in

BM cell-free fluids of saline-, TPO^{high} plus vehicle–, and TPO^{high} plus TAK-242–treated mice. **(P)** Representative spleens from treated mice. **(Q)** Quantification of spleen/body weight ratios in saline-, TPO^{high} plus vehicle–, and TPO^{high} plus TAK-242–treated mice. n = 6. **(R–T)** Peripheral platelet (PLT; R), white (WBC; S), and red blood cell (RBC; T) counts of treated mice. n = 6. *, P < 0.05; **, P < 0.01; ***, P < 0.001. Data are shown as mean ± SD.

hyperplasia were less marked in *Tlr4*$^{-/-}$ mice (Fig. 6, B–G). Decline of BM erythropoiesis was less evident in *Tlr4*$^{-/-}$ mice (Fig. S4 F) as well as the increase in splenic erythropoiesis (Fig. S4 G). Moreover, fewer colonies developed from *Tlr4*$^{-/-}$ BM and spleens with respect to *wt/wt* mice (Fig. S4, H and I). Of note, in this model, TLR4 deletion was sufficient to abrogate the rise of BM IL-6, while TNF-α level was unchanged as in the control *wt/wt* mice (Fig. 6, H and I). In *wt/wt* mice, the rise of IL-6 was particularly evident in CD41^{+} Mk's, which displayed higher mean fluorescence intensity of IL-6 expression, but not of TNF-α, after experimental fibrosis (Fig. 6, J–L). On the contrary, Mk's of *Tlr4*$^{-/-}$ mice did not show increased expression of either (Fig. 6, J–L). In keeping with these results, BM fibrosis was strongly attenuated by TLR4 depletion (Fig. 6, M and N), as well as FN and type III collagen deposition (Fig. 6, O and P). Interestingly, spleen size (Fig. 6, Q and R) and extramedullary hematopoiesis (Fig. 6 S) were significantly decreased in *Tlr4*$^{-/-}$ mice. Moreover, thrombocytosis, leukocytosis, and anemia were mildly attenuated in *Tlr4*$^{-/-}$ mice (Fig. 6, T–V). Finally, we employed *EIIIA*$^{+/+}$*/TLR4*$^{-/-}$ mice, which constitutively express EDA FN but lack TLR4, and *EIIIA*$^{-/-}$*/TLR4*$^{-/-}$ mice, which lack both EDA FN and TLR4 (Fig. 7 A). TPO treatment of mice with forced expression of EDA domain in the absence of TLR4, as well as in double knockout mice, recapitulated the low fibrotic phenotype of *Tlr4*$^{-/-}$ mice in terms of Mk hyperplasia (Fig. 7, B–E), reticulin deposition (Fig. 7, F and G), and spleen size (Fig. 7, H and I).

Expression of EDA FN in the hematopoietic tissues of patients with PMF

It is known that in PMF patients, Mk's express and release an increased level of TGF-β that induces BM fibrosis (Ciurea et al., 2007; Badalucco et al., 2013). Therefore, we analyzed the impact of TGF-β in modulating EDA FN expression and splicing in human BM-derived MSCs. After 24 h of TGF-β stimulation (10 ng/ml), we observed an increased expression of EDA FN at both molecular (Fig. 8 A) and protein levels (Fig. 8, B and C).

We then determined the expression levels of EDA FN in patients with PMF. Analysis of BM biopsies (BMBs) of PMF patients at different phases of fibrosis (grade 0 to 3 according to WHO classification), with a monoclonal antibody directed to the EDA domain, demonstrated that this isoform is almost undetectable in BMBs of healthy controls (HCs; Fig. 8 D, upper panel I), but significantly increased in PMF patients presenting higher grades of BM fibrosis (Fig. 8 D, upper panels II–V; and Fig. 8 E). On the contrary, total FN was present in BMBs of HCs (Fig. 8 D, lower panel I) and throughout fibrotic development (Fig. 8 D, lower panels II–V).

Levels of circulating EDA FN were measured in plasma samples through an immunoassay developed by our group. Potential cross-reactions of the newly established ELISA assay with human pFN lacking EDA domain (Fig. S5 A) or with components of the test system were serially excluded (Fig. S5 B). A cross-sectional evaluation of circulating EDA FN was performed in 105 subjects with PMF. 37 subjects were analyzed at diagnosis and 68 after the diagnosis (median time from diagnosis, 73 mo; range, 7–289 mo). Demographic, clinical, and biological features of the study population are reported in Table 1. Levels of circulating EDA FN in plasma samples of patients with PMF had a mean value of 5.92 µg/ml (median, 3.92; range, 0.42–21.46). HCs (n = 15) had a range of values from 0.85 to 5.32 µg/ml with a mean value of 2.96 µg/ml. PV and ET patients together (n = 22) had a mean value of EDA FN in plasma of 2.60 µg/ml (median, 2.23; range, 0.42–7.56). Circulating EDA FN in PMF patients was higher than in HCs (Mann-Whitney U test, P = 0.028) and in PV/ET subjects (P = 0.001). No significant difference was revealed in circulating EDA FN between PV/ET patients and HCs (P = 0.39; Fig. 8 F). Further, we found a difference in plasma levels of EDA FN among patients with different degrees of BM fibrosis. The analysis showed a trend of increasing levels of circulating EDA FN with increasing BM fibrosis grades; however, the association between EDA FN plasma levels and the degrees of BM fibrosis was not statistically significant. By grouping patients with prefibrotic myelofibrosis (BM fibrosis grade 0) together with those with early myelofibrosis (BM fibrosis grade 1; early fibrosis; n = 30; median, 3.61; range, 1.16–21.46) and those with BM fibrosis grade 2 together with those with BM fibrosis grade 3 (advanced fibrosis; n = 8; median, 7.61; range, 2.87–10.99), the difference of circulating EDA FN in plasma was statistically significant (P < 0.05; Fig. 8 G). Overall, these data demonstrated that patients with PMF display higher levels of the EDA FN isoform with respect to HCs.

Discussion

BM fibrosis is characterized by progressive deposition of reticulin, FN, and collagen fibers that leads to disruption of the tissue architecture. A role for TGF-β in the development of BM fibrosis has been widely proposed (Vannucchi et al., 2005; Zingariello et al., 2013; Ceglia et al., 2016; Dutta et al., 2017). TGF-β can be produced by cells within the megakaryocytic lineage in myelofibrosis patients and in macrophages (Ciurea et al., 2007). The fibrogenic activity of TGF-β modulates the alternative splicing of the FN gene, leading to protein diversity (Han et al., 2007). Among the ECM proteins that fill the BM cavity, FN has a complex pattern of alternative splicing at the mRNA level that allows several forms of FN whose expression has been proven to be altered in tumors (Oyama et al., 1990). The involvement of EDA FN in important pathological processes such as atherosclerosis (Doddapattar et al., 2015), lung fibrosis (Muro et al., 2008), and liver fibrosis (Jarnagin et al., 1994) has been well described. On the contrary, its effect on the hematopoietic tissue has been poorly studied (Malara et al., 2018).

In this work, higher expression levels of EDA FN were detected in endothelial and stromal cells after experimental

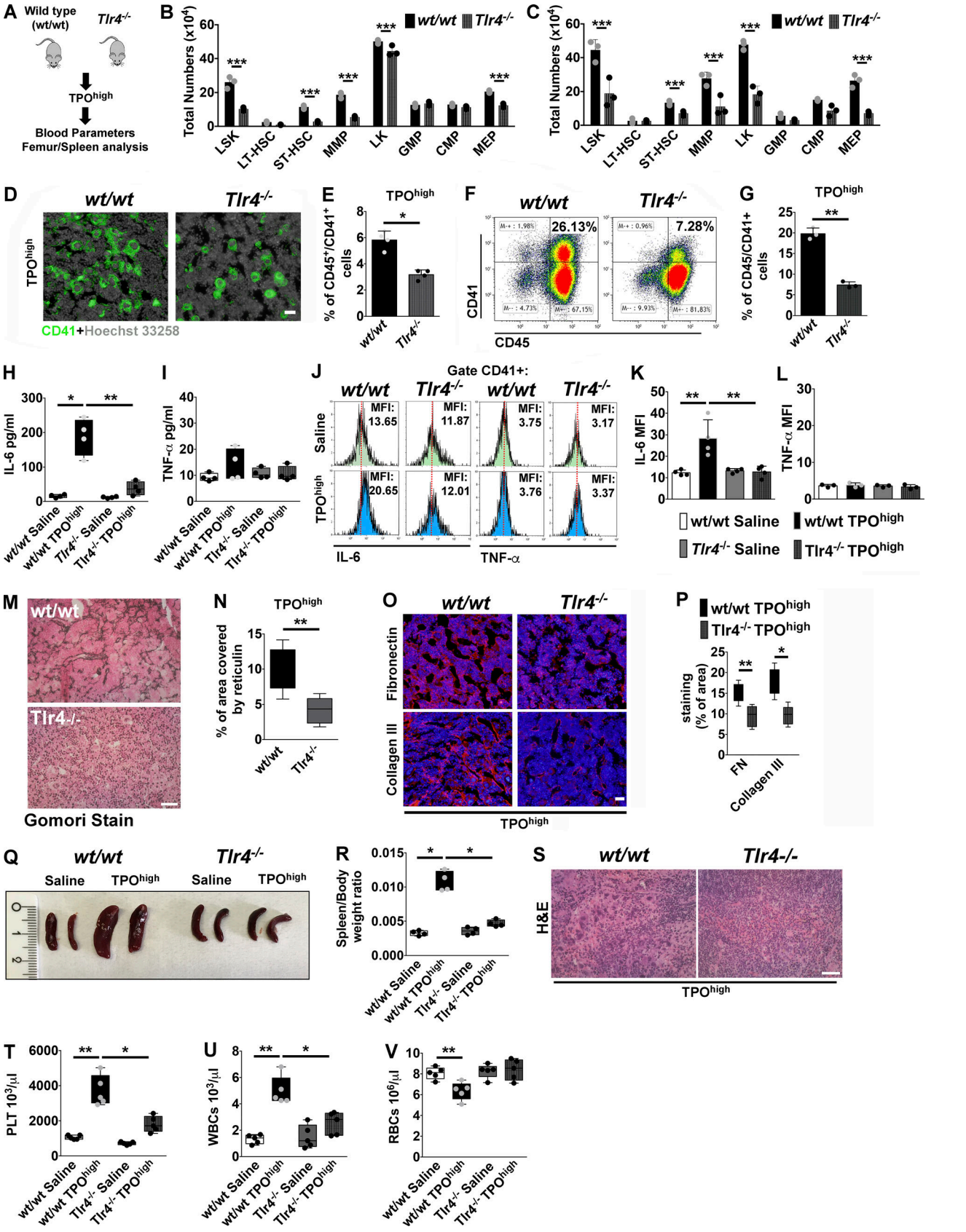

Figure 6. **TLR4 deletion protects from experimental BM fibrosis in mice. (A)** The TPO^{high} model was established in *wt/wt* and *Tlr4*$^{-/-}$ mice. **(B and C)** Total numbers of LSK, LT-HSC, ST-HSC, MMP, CMP, GMP, and MEP cells in the BM (B) and spleens (C) of *wt/wt* and *Tlr4*$^{-/-}$ mice after treatment with TPO. $n = 3$. **(D)** Immunofluorescence of BM CD41^{+} Mk's in *wt/wt* and *Tlr4*$^{-/-}$ mice after treatment with TPO. Nuclei were stained with Hoechst 33258. Bar, 50 µm. Objective,

20×. **(E)** Flow cytometry quantification of CD45/41⁺ Mk's in BM cells of *wt/wt* and *Tlr4*$^{-/-}$ mice after treatment with TPO. *n* = 4. **(F and G)** Flow cytometry analysis of CD45/41⁺ Mk's (F) and relative quantification (G) in spleen cells of *wt/wt* and *Tlr4*$^{-/-}$ mice after treatment with TPO. *n* = 3. **(H and I)** Quantification of IL-6 (*n* = 7; H) and TNF-α (*n* = 6; I) in BM cell-free fluids of *wt/wt* and *Tlr4*$^{-/-}$ mice treated with TPO. **(J–L)** Flow cytometry histograms (J) and relative mean fluorescence intensity (MFI) quantification of intracellular IL-6 (K) and TNF-α (L) of CD41⁺ Mk's in saline and TPO treated *wt/wt* and *Tlr4*$^{-/-}$ mice. *n* = 3. **(M and N)** Representative Gomori stain (M) and quantitative assessment of reticulin deposition (N) in BM sections of *wt/wt* and *Tlr4*$^{-/-}$ mice after experimental fibrosis. Bar, 50 µm. Objective, 20×. *n* = 3. **(O and P)** Immunofluorescence staining (O) and quantitative assessment (P) of FN and type III collagen in BM sections of *wt/wt* and *Tlr4*$^{-/-}$ mice after experimental fibrosis. Bar, 50 µm. Objective, 60×. **(Q)** Representative spleens of saline and TPO treated *wt/wt* and *Tlr4*$^{-/-}$ mice. **(R)** Spleen/body weight ratios in *wt/wt* and *Tlr4*$^{-/-}$ mice treated with saline or TPO. *n* = 4. **(S)** H&E stain of spleen sections of *wt/wt* and *Tlr4*$^{-/-}$ mice after experimental fibrosis. Bar, 50 µm. **(T–V)** Peripheral platelet (PLT; T), white (WBC; U), and red blood (RBC; V) cell counts of *wt/wt* and *Tlr4*$^{-/-}$ mice after TPO treatment. *n* = 5. *, P < 0.05; **, P < 0.01; ***, P < 0.001. Data are shown as mean ± SD.

fibrosis, in line with recent work, by our group and others, that demonstrated increased level of FN expression in BM-derived MSCs and osteoblasts from patients with PMF with respect to HCs (Schneider et al., 2014; Abbonante et al., 2016b). To definitely unravel the role of EDA segment on fibrotic progression in vivo, we exploited two unique transgenic mouse models that present an aberrant splicing of the EDA exon (EIIIA in mice; Muro et al., 2003). At the opposite from the knockout mice (EIIIA$^{-/-}$), mice with constitutive inclusion of EDA exon in tissues were more prone to BM fibrosis development as suggested by extensive reticulin deposition, thrombocytosis, splenomegaly, and increased extramedullary hematopoiesis after TPO challenge.

Differently from other tissues, most diseases with increased BM fibrosis are associated with abnormalities of the number and/or function of Mk's. Although the molecular identity of the receptor remains still elusive, the EDA segment of FN has been identified as a potential damage-associated molecular pattern, based on its ability to activate TLR4 (Okamura et al., 2001). By several in vitro approaches, we demonstrated that cellular EDA FN, but not pFN lacking the EDA domain, induces hematopoietic progenitor cell proliferation and Mk differentiation through engagement of TLR4 and activation of STAT-5 and ERK 1/2 signaling pathways. Several pieces of evidence demonstrated that TLR4 activation by its natural agonist, LPS, in addition to NF-κB and ERK 1/2 activation, results in a direct interaction (and activation) of JAK-2 and STAT-5 with TLR4 inducing the secretion of IL-6 by macrophages (Kimura et al., 2005). Here we report that EDA FN induces a similar activation status in Mk's, as significant phosphorylation of STAT-5 in a TPO-independent manner was achieved after incubation with EDA FN, which was abolished by pharmacological inhibition of TLR4 through the inhibitor TAK-242. Importantly, the concomitant treatment in vivo of the TPO^{high} mouse model with the TLR4 inhibitor TAK-242, or induction of BM fibrosis in *Tlr4*$^{-/-}$ mice, brought all the fibrotic features such as Mk hyperplasia, BM reticulin

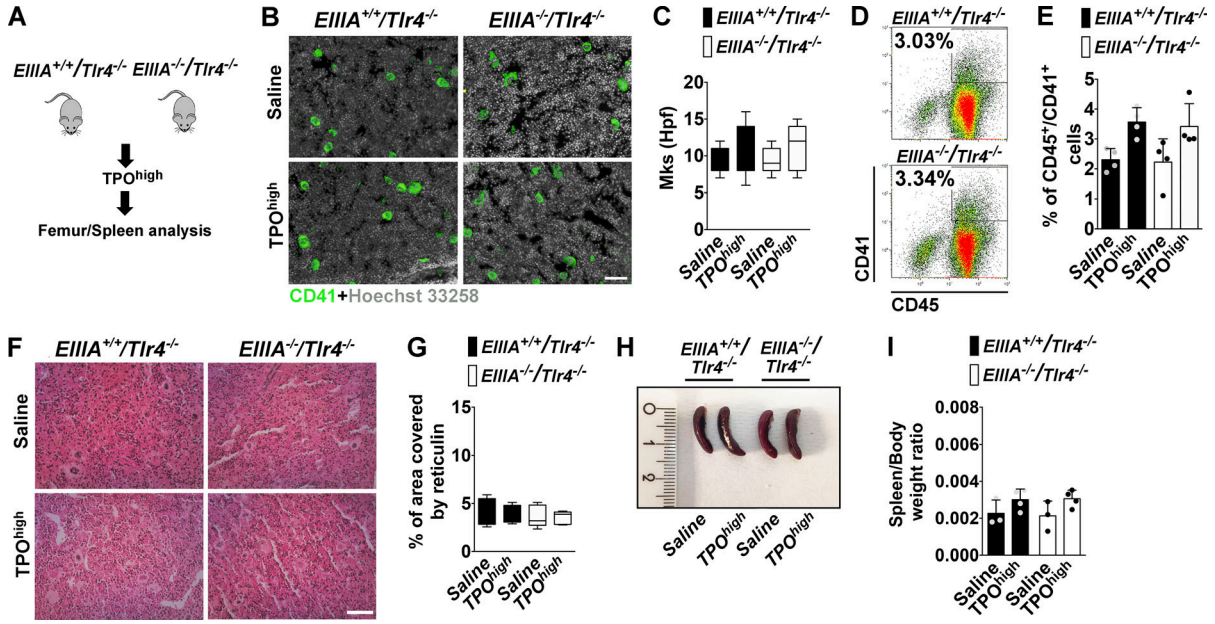

Figure 7. **Response of EIIIA$^{+/+}$/Tlr4$^{-/-}$ and EIIIA$^{-/-}$/Tlr4$^{-/-}$ mice to TPO confirmed the critical role of EDA FN–TLR4 axis in BM fibrosis. (A)** The TPO^{high} model was established in *EIIIA*$^{+/+}$*/Tlr4*$^{-/-}$ and *EIIIA*$^{-/-}$*/Tlr4*$^{-/-}$ mice. **(B and C)** Representative immunofluorescence of BM CD41⁺ Mk's (B) and quantification of Mk's per high power field (hpf; C) in *EIIIA*$^{+/+}$*/Tlr4*$^{-/-}$ and *EIIIA*$^{-/-}$*/Tlr4*$^{-/-}$ mice after treatment with TPO. Bar, 50 µm. Objective, 20×. **(D and E)** Representative flow cytometry dot plots (D) and relative quantification (E) of CD45/41⁺ Mk's in BM cells of *EIIIA*$^{+/+}$*/Tlr4*$^{-/-}$ and *EIIIA*$^{-/-}$*/Tlr4*$^{-/-}$ mice after treatment with TPO. *n* = 4. **(F and G)** Gomori stain (F) and quantitative assessment of reticulin deposition (G) in treated mice. Bar, 50 µm. Objective, 20×. *n* = 3. **(H)** Representative spleens of saline- and TPO-treated *EIIIA*$^{+/+}$*/Tlr4*$^{-/-}$ and *EIIIA*$^{-/-}$*/Tlr4*$^{-/-}$ mice. **(I)** Quantification of spleen/body weight ratios in *EIIIA*$^{+/+}$*/Tlr4*$^{-/-}$ and *EIIIA*$^{-/-}$*/Tlr4*$^{-/-}$ mice treated with saline or TPO. *n* = 3 and 4, respectively. *, P < 0.05; **, P < 0.01; ***, P < 0.001. Data are shown as mean ± SD.

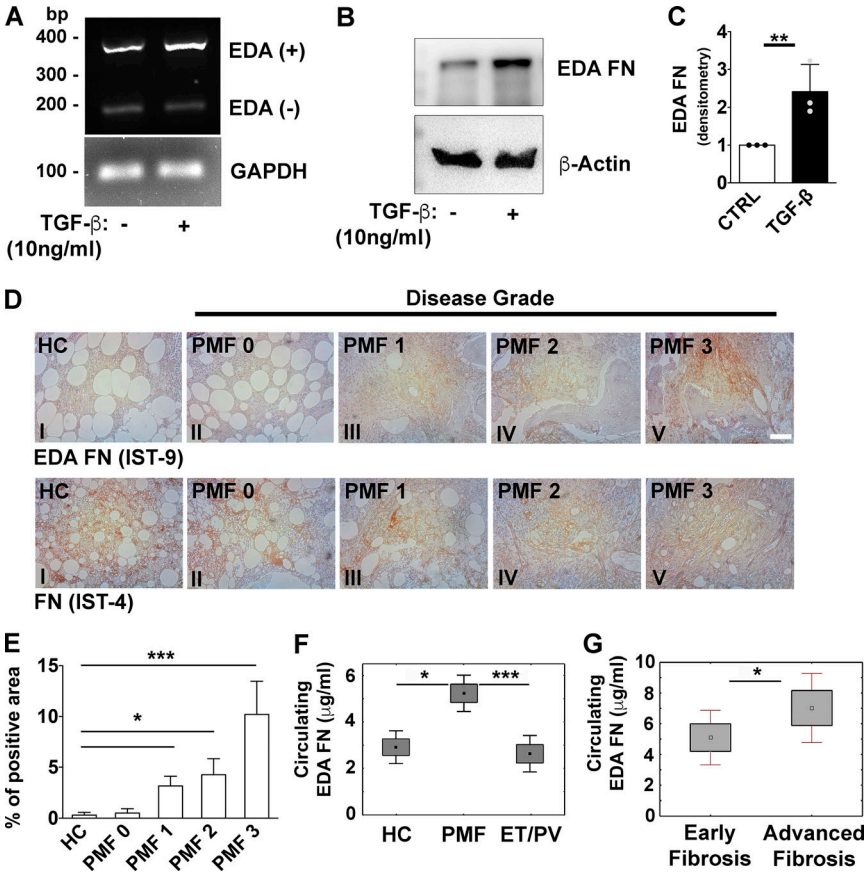

Figure 8. **Increased release of FN containing EDA domain during fibrotic progression in PMF patients. (A)** Human BM-derived MSCs were stimulated for 24 h with 10 ng/ml of recombinant human TGF-β. Splicing of alternative EDA exon was analyzed by PCR assay. GAPDH was used for comparative concentration analysis. **(B and C)** Representative Western blot (B) and relative quantification (C) of EDA FN expression in MSCs stimulated or not with TGF-β. β-Actin was revealed to ensure equal protein loading. *n* = 3. Data are shown as mean ± SD. **(D)** Stains of FN containing EDA segment (Ab IST-9; upper panels, I–V) in BMBs of HC (upper panel I, *n* = 3) and PMF patients at grade 0, 1, 2, and 3 of BM fibrosis (upper panels II–V, respectively). Stains of total FN in the same specimens are shown in lower panels I–V. Bar, 100 µm. **(E)** EDA FN staining expressed as percent of positive area in HC and PMF at different phases of disease (*n* = 3 per each phase). Data are shown as mean ± SD. **(F)** Values of circulating EDA FN (µg/ml in 500 µg/ml of total pFN; mean ± 1.96 SE) in plasma samples of subjects stratified according the diagnosis (PMF: *n* = 105; PV: *n* = 6; ET: *n* = 16; or HC: *n* = 15). **(G)** Circulating plasma EDA FN (mean ± 1.96 SE) in PMF patients according to their phase of fibrotic disease: early BM fibrosis (grade 0/1, *n* = 30) or advanced BM fibrosis (grade 2/3, *n* = 8). *, P < 0.05; **, P < 0.01; ***, P < 0.001.

deposition, splenomegaly, and the increased cytokine release back to control levels. Consistently, double transgenic mice, *EIIIA*$^{-/-}$*/Tlr4*$^{-/-}$, and *EIIIA*$^{+/+}$*/Tlr4*$^{-/-}$ did not develop extensive fibrosis after TPO treatment.

Table 1. **Demographic and clinical features of patients with PMF at the time of blood sampling for EDA FN plasma determination**

Parameters	Total population
Number	105
Females, *n* (%)	56 (53.3)
Age at onset of the disease, yr, median (range)	49 (27–80)
Hemoglobin, g/liter, median (range)	12.9 (7.3–17.8)
White blood cell count, ×10^9/liter, median (range)	7.8 (1.4–28.3)
Immature myeloid cells in peripheral blood, %, median (range)	0 (0–13)
Blasts in peripheral blood, %, median (range)	0 (0–6)
Platelet count, ×10^9/liter, median (range)	363 (48–1,184)
Spleen index, cm^2, median (range)[a]	120 (90–665)
CD34$^+$, ×10^6/liter, median (range)	9.6 (0.6–1,339)
LDH (× ULN)	1.19 (0.5–2.5)

LDH, lactate dehydrogenase; ULN, upper limit of normal.
[a]Spleen index is the product of the longitudinal by the transversal spleen axis, the latter defined as the maximal width of the organ.

The alternatively spliced segment EDA and partially unfolded III-1 domain, FNIII-1c, were demonstrated to induce the expression of multitude of proinflammatory cytokines in human dermal fibroblasts (Kelsh et al., 2014). Therefore, the ability of the EDA segment of FN to induce a proinflammatory phenotype in Mk's was also investigated in our research. Our results confirmed that stimulation of Mk's with EDA FN resulted in increased synthesis of proinflammatory cytokines in a TLR4-dependent manner. Particularly, EDA FN induced the Mk production of IL-6 but not of TNF-α.

Interestingly, opposite effects have been attributed to these cytokines during fibrotic progression: IL-6 is identified as a profibrotic cytokine that stimulates ECM protein release, and it is known to increase NF-κB and STAT3 activation, causing inhibition of apoptosis and increased myeloproliferation, hence creating an environment favorable to malignant transformation and expansion (Hasselbalch, 2013; Fielding et al., 2014), while TNF-α acts as an anti-fibrotic cytokine by inhibiting type I and type III collagen and FN expression in several cell types (Mauviel et al., 1988; Mori et al., 2002). Further, their effects are opposite also on megakaryopoiesis, with IL-6 acting as key regulator of megakaryopoiesis (Wu et al., 2015), while TNF-α acts as a potent inhibitor of this process (Kaushansky, 2005). Thus, EDA FN might represent a new regulator mediating ECM deposition and inflammatory responses, which are corollaries of the fibrotic process in vivo. EIIIA mice models were previously employed to study the role of cFN in a variety of organs, including lung and skin, under fibrotic conditions. EIIIA$^{-/-}$ were protected from

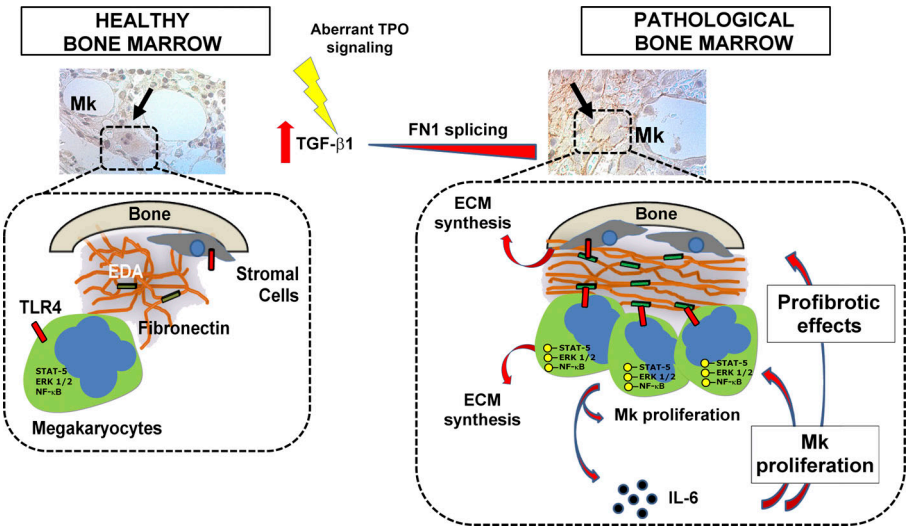

Figure 9. **Role of EDA FN during BM fibrosis.** In HCs, very low levels of EDA domain are included in the FN matrix and are unaccessible to TLR4 on cell surface. During fibrotic development, Mk proliferation and TGF-β1 released from pathological cells might induce an up-regulation of EDA exon splicing in the surrounding niche cells. EDA FN is then released in the extracellular space, where it engages TLR4 on hematopoietic progenitor cell surface concurring to the activation of signaling pathways related to Mk proliferation and differentiation. Further, EDA FN–dependent activation of NF-κB results in the release of profibrotic cytokines that, in turn, may further enhance the release of ECM as well as the proliferation of different BM cellular components. The ensuing positive feedback loop is likely to contribute to the persistence and progression of fibrosis.

bleomycin-induced lung fibrosis (Muro et al., 2008) or allergen-induced airway fibrosis (Kohan et al., 2011). Similarly, genetic ablation of EDA FN or TLR4 blockade mitigated the induced cutaneous fibrosis in mice (Bhattacharyya et al., 2014). In this scenario, our data represent the first experimental evidence of an increased predisposition of the EIIIA$^{+/+}$ mice to fibrotic evolution. Overall, these data suggest that an EDA^{+} environment seems to recreate the most permissive setting for fibrosis development through the engagement of TLR4.

Most importantly, based on these data, we showed that, at variance with HCs, patients with PMF display increased levels of EDA FN in plasma and BMBs during fibrotic progression. The use of plasma levels of cellular isoforms of FN as a disease biomarker has previously been explored in several solid tumors with controversial results (Ylätupa et al., 1995). Our analysis on circulating and tissue levels of EDA FN in PMF patients demonstrated that EDA FN expression increases in the plasma and BM of advanced fibrotic PMF patients, suggesting that EDA FN plays a role in the pathogenesis and/or may be used as a biomarker in MPNs.

In conclusion, we demonstrated that increased expression of alternatively spliced isoform of FN containing EDA domain is observed during BM fibrosis progression and that the EDA–TLR4 axis sustains the expansions of Mk's with a proinflammatory phenotype. This, in turn, may concur to alter the BM environment, rendering it more permissive to the characteristic Mk proliferation observed in patients with BM fibrosis (Fig. 9). Overall, EDA segment and TLR4 targeting might represent new potential therapeutic approaches in patients with high-grade myelofibrosis.

Materials and methods

Animals

All animal studies were reviewed and approved by the Italian Ministry of Health (approval 3/2013, 1302/2015, and 990.2017-PR/2017). All animals were sacrificed according to the current European legal Animal Practice requirements. Wild-type mice C57BL/6J mice were from Charles River Laboratories. EIIIA$^{+/+}$ and EIIIA$^{-/-}$ mouse strains were previously generated (Muro et al., 2003). Tlr4$^{-/-}$, EIIIA$^{+/+}$/Tlr4$^{-/-}$, and EIIIA$^{-/-}$/Tlr4$^{-/-}$ mouse strains were previously described (Doddapattar et al., 2015). All the mice used in the present study were bred in-house and were on a C57BL/6J background. Mice were housed at the animal facility of the Department of Physiology, section of General Physiology, University of Pavia, Pavia, Italy. For the establishment of the TPO^{high} mouse model, 6–8-wk-old wild-type, EIIIA$^{+/+}$, EIIIA$^{-/-}$, TLR4$^{-/-}$, EIIIA$^{+/+}$/Tlr4$^{-/-}$, and EIIIA$^{-/-}$/Tlr4$^{-/-}$ mice received subcutaneous injections of either vehicle (saline, PBS) or romiplostim (100 µg/kg of body weight; Amgen) every 3 d for 1 mo. Doses and administration schedules were selected according to previous studies in mice (Kuter et al., 2009; Léon et al., 2012). TLR4 inhibitor (TAK-242; 1 mg/kg of weight) was injected intraperitoneally every day for 1 mo according to previous studies in mice (Khan et al., 2012; Wang et al., 2016a,b). DMSO was injected as vehicle in saline solution (5% vol/vol). Blood samples were analyzed for blood count at baseline and at day 30 of treatment on a Cell Dyn 3700 hematology analyzer (Abbott Diagnostics). At day 30, mice were killed, and organs (spleen and BM) were removed and immersed in 4% paraformaldehyde or optimal cutting temperature compound for histological/immunofluorescence analysis.

Study population

All studies using human tissues were reviewed and approved by the Institutional Review Boards at the Istituto di Ricovero e Cura a Carattere Scientifico Policlinico S. Matteo Foundation, Pavia, Italy, and received patients' informed consent. We obtained EDA FN plasma concentration values and health care data of patients with PMF from the database of the Center for the Study of Myelofibrosis at the Istituto di Ricovero e Cura a Carattere Scientifico Policlinico S. Matteo Foundation. The database prospectively collects information of all consecutive PMF patients who had a first-ever encounter at the center (at the cut-off date of July 31, 2017; n = 956). For the present study, we selected all patients who had provided written informed consent for plasma sample collection as well as for participation in research studies related to their disease. We then sequentially excluded, in

descending order, patients who had been treated with disease-modifying agents at any time before or on the date of base-cohort entry (hydroxyurea, interferon, ruxolitinib, corticosteroids, immunosuppressive agents, danazol), and patients with the following concomitant diseases: acute inflammatory disease, autoimmune disease, other malignancies, severe liver dysfunction, and severe renal dysfunction. The control population was composed of 15 healthy subjects matched for age and gender, 16 patients with ET, and 6 with PV.

All the patients entering the database had the diagnosis of PMF confirmed by the revision of the BMB samples by an expert pathologist according the 2008 WHO criteria. Clinical data at diagnosis of all the patients and morphological features were reexamined and classified according to the WHO 2016 criteria. The clinical characteristics of the subjects are shown in Table 1.

Blood was drawn into whole blood tubes with 0.106 mol/liter buffered sodium citrate (ESR 4 NC/2 ml; Sarstedt S-MonovetteR) with a 4:1 blood to anticoagulant ratio. The plasma was immediately separated from the blood cells by centrifugation at 2,000 *g* for 10 min. The samples were stored in 500 µl aliquots at −76°C until analysis. Frozen samples were thawed for 1 h at room temperature (20°C) before use.

Antibodies and reagents

LPS from *Escherichia coli* serotype 0111:B4 and cFN from skin fibroblasts were from Sigma-Aldrich. TAK-242, TLR1/2 agonist Pam_3Csk_4, and TLR9 agonist CpG ODNs were purchased from Invivogen. pFN was from BD Bioscience. The following antibodies were used: anti-FN was from Chemicon (Merck-Millipore), and anti–EDA FN (FN-3E2), anti-FN (FN IST-4), and anti–β-actin were all from Sigma-Aldrich. Anti–EDA FN (IST-9) and anti–type III collagen were from Abcam. Anti–β3 integrin, anti-TLR4 (clone 25 and M-300), and anti-α4 (clone C19) were from Santa Cruz Biotechnology. Anti-mouse CD49d (α4 integrin) with blocking function was from BioLegend (clone 9C10). Anti–phospho-ERK 1/2, anti-ERK 1/2, anti–phospho–STAT-5, anti–STAT-5, anti–phospho p65 (NF-κB), and p65 (NF-κB) were purchased from Cell Signaling Technologies. EDA^+ and EDA^- recombinant peptides were produced as previously described (Losino et al., 2013). All the experiments were performed with the same batch for each peptide.

Tissue specimen collection

BMBs of patients were available from previous studies (Abbonante et al., 2016a). Normal control samples were age-matched BMB specimens obtained for staging purposes that were determined to be free of neoplasia and other abnormalities upon histological and immunohistochemical examination. BMBs were formalin-fixed, decalcified, and paraffin-embedded. Mouse femurs and spleens were removed from 6–8-wk-old mice and fixed for 24 h in 3% paraformaldheyde or 4% buffered formalin. Bones were decalcified in a solution of 10% EDTA, in PBS (without calcium and magnesium), pH 7.2, for 2 wk at 4°C. Spleens and bones were embedded in optimal cutting temperature compound cryo-sectioning medium and snap-frozen in a chilling bath or alternatively paraffin-embedded. 5-µm tissue sections were taken by using a Microm Microtome HM 250 (Bio-Optica) and processed for fluorescence microscopy or immunohistochemistry.

Immunofluorescence

Frozen sections were fixed for 20 min in 4% paraformaldheyde, washed with PBS, and blocked with 2% BSA (Sigma-Aldrich) in PBS for 30 min. Unspecific binding sites were saturated with 5% goat serum, 2% BSA, and 0.1% glycine in PBS for 1 h. FITC-conjugated anti-CD41 was diluted 1:100, anti-FN 1:500, and anti–type III collagen 1:100 and incubated overnight at 4°C in washing buffer (0.2% BSA, 0.1% Tween 20 in PBS). 594 Alexa Fluor–conjugated secondary antibodies were purchased from Invitrogen. Nuclei were counterstained using Hoechst 33258 (100 ng/ml in PBS) at room temperature. Sections were then mounted with micro-cover glasses using Fluoro-mount (Bio-Optica). Negative controls were routinely performed by omitting the primary antibodies. Images were acquired using the Olympus BX51 fluorescence microscopy (Olympus Deutschland) and 10×/0.30 or 20×/0.75 Olympus UplanF1 objectives or with a TCS SP8 confocal laser scanning microscope (Leica).

ELISAs

BM cells were obtained by flushing mice femurs with 1 ml of PBS. Cells were centrifuged at 15,700 *g* and the cell-free fluids (BM supernatants) collected. After measuring protein content with bicinchoninic acid assay, supernatants were used for determination of TNF-α and IL-6 with commercially available mouse ELISA kits according to the manufacturer's instructions (BioLegend). Quantification of total FN in plasma samples was performed with a commercially available kit according to the manufacturer's instructions (HFN1; Thermo Fisher Scientific). Plasma samples were then diluted to achieve a FN concentration of 500 µg/ml in each sample. Circulating EDA FN was measured with an ELISA developed by our group. Briefly, the concentrations of EDA FN in plasma were measured using 96-well micro-titration plates (high binding; Elisa Max; BioLegend). The strips were coated overnight with IST-9 antibody (1 µg/well; specific for EDA FN; Abcam) and washed four times with 0.02 mol/liter PBS (pH 7.0) containing 0.1% Tween 20. Thereafter, 100 µl of plasma sample or standard was added and incubated for 1 h at 37°C. The unbound material was removed with the above washing buffer, and a polyclonal antibody anti-FN (gift from Professor Livia Visai, Department of Molecular Medicine, University of Pavia, Pavia, Italy; Speziale et al., 2008), diluted 1:3,000, was added to wells. After incubation at 37°C for 1 h, the strips were washed, and 100 µl of peroxidase-conjugated antibody (Bio-Rad) was added for an additional hour to wells. Bound enzyme activity was visualized by adding 100 µl of substrate solution containing hydrogen peroxide and tetramethylbenzidine (BioLegend). Substrate incubation was allowed to proceed for 30 min, after which the reaction was stopped with 100 µl of 4 mol/liter H_2SO_4. Absorbances were measured in a Bio-Rad microtitration plate reader at 450 nm. Reproducibility of the EDA FN assay was judged by five repeated assays of eight EDA FN standard stocks (8, 4, 2, 1, 0.5, 0.25, 0.125, and 0 µg/ml) and samples of plasma. The inter-assay coefficient of variation of a standard (1.0 µg EDA FN per milliliter) measured in 96

microtiter plates was 6.1%, and the intra-assay coefficient of variation was 4.0%. An amount of 0.3 µg/ml in plasma could be detected in the linear range of the standard curve. Human FN standard containing EDA domain was isolated from human skin fibroblasts (Sigma-Aldrich).

Western blotting

Cells were lysed in Hepes-glycerol lysis buffer (50 mM Hepes, 150 mM NaCl, 10% glycerol, 1% Triton X-100, 1.5 mM $MgCl_2$, and 1 mM EGTA) containing 1 µg/ml leupeptin and 1 µg/ml aprotinin for 30 min at 4°C. Samples were clarified by centrifugation at 15,700 *g* at 4°C for 15 min. Protein content in BM cell-free fluids was analyzed by bicinchoninic acid assay after clarification. Laemmli sample buffer was then added to supernatants. Samples were always heated at 95°C for 3 min, separated by electrophoresis on 12% sodium dodecyl sulfate-polyacrylamide gel, and then transferred to polyvinylidine fluoride membranes. Membranes were probed with primary antibodies, washed three times with PBS and Tween 0.1%, and incubated with an appropriate peroxidase-conjugate secondary antibody. Membranes were visualized using Immobilon Western chemiluminescent HRP substrate (Millipore) and ChemiDoc XRS Imaging System (Bio-Rad).

Immunoprecipitation

Co-immunoprecipitation of FN with endogenously expressed proteins was performed on differentiated mouse Mk's. Cells were harvested in Hepes-glycerol lysis buffer, and extracts were incubated overnight with 2.5 µg of anti-TLR4 (M-300) or anti–α4 integrin (all from Santa Cruz Biotechnology) in the presence of Protein A/G PLUS agarose beads (Santa Cruz Biotechnology), and resulting complexes were washed, denatured, and eluted according to the manufacturer's instructions. Mouse anti-TLR4 (25; Santa Cruz Biotechnology) was used to highlight TLR4 immunoprecipitation. Mouse anti–EDA FN (clone FN3E2; Sigma-Aldrich) was used to detect coimmunoprecipitated FN.

PCR and real-time PCR

Retrotranscription (RT) was performed in a final volume of 20 µl reaction using the iScriptTM cDNA Synthesis Kit according to the manufacturer's instructions (Bio-Rad). For quantitative real-time PCR, RT samples were diluted up to 60 µl with bidistilled H_2O, and 3 µl of the resulting cDNA was amplified in triplicate in 15 µl reaction mixture with 200 nM of each specific primer and SsoFast Evagreen Supermix (Bio-Rad) at 1× as final concentration. The amplification reaction was performed in a CFX Real-time system (Bio-Rad) as follows: 95°C for 5 min, followed by 35 cycles at 95°C for 10 s, 60°C for 15 s, and 72°C for 20 s. Primers compassing the specific EIIIA exon of FN were as follows: forward, 5′-CCCTAAAGGACTGGCATTCA-3′; and reverse, 5′-CAT CCTCAGGGCTCGAGTAG-3′. Pre-designated KiCqStart primers for human GAPDH and mouse IL-6, TNF-α, TLR2, TLR9, ITGA4, ITGA5, ITGA9, ITGAV, and β2-microglobulin genes were purchased from Sigma-Aldrich. The Bio-Rad CFX Manager software 3.0 was used for the normalization of the samples. β2-microglobulin gene expressions were used for the comparative concentration analysis. PCR splicing assays for human and mouse EDA, mouse EDB, and V region were performed as previously described (Malara et al., 2011, 2016).

Flow cytometry

For LSK cell analysis, cells were stained for 30 min on ice with antibodies against c-Kit (clone 2B-8), Sca-1 (clone D7), CD16/32 (FcγR II/III; clone 93), Flk2 (CD135; clone A2F10; all from eBioscience), CD34 (clone RAM34; BD Biosciences), and antibodies against Lin markers (Miltenyi Biotech). For erythroid progenitor cells analysis, BM and spleen cells were stained with antibodies against CD71 (clone R17217) and Ter119 (clone Ter119; all from eBioscience). FITC-BrdU Flow Kit was purchased from BD Pharmingen. BM-differentiated Mk's were stained with PE-conjugated anti-mouse CD41 (clone MWReg30; BioLegend). For quantification of BM Mk's frequencies, BM cells were stained with anti–CD41-PE and anti–CD45-FITC (Miltenyi Biotech). For intracellular staining of cytokines, BM cells were fixed and permeabilized with BD Citofix/Citoperm fixation and permeabilization solution (BD Biosciences) and stained with CD41-PE, anti–IL-6 FITC (clone MP5-20F3; BioLegend) and anti–TNF-α APC (clone MP6-XT22; BioLegend). 7-aminoactinomycin D solution (BD Pharmingen) was used for cell survival analysis. All the samples were acquired with a Beckman Coulter FacsDiva flow cytometer. Non-stained samples and relative isotype controls were used to set the correct analytical gating. Off-line data analysis was performed using a Beckman Coulter Kaluza version software package.

Colony-forming assays

BM (10^4) and spleen (10^5) cells were plated in duplicates in cytokine-supplemented complete methylcellulose medium (MethoCult M3434; Stemcell Technologies). BFU-E, CFU-GM, and granulocyte-erythrocyte-macrophage-Mk (CFU-GEMM) colonies were scored on day 7 according to the manufacturer's protocol.

Immunohistochemisty and Gomori staining

Formalin-fixed, paraffin-embedded human BMB specimens from HCs and PMF patients were obtained from the posterior superior iliac spine and decalcified using an EDTA-based solution for 72 h. Immunohistochemistry was performed using an automated staining system (BenchMark ULTRA; Ventana; Roche). Heat-induced antigen retrieval was automatically obtained using a 0.05 mol/liter EDTA solution, pH 8.0, at 95°C for 30 min. Reactions were revealed using ultraView Universal DAB Detection Kit (Ventana; Roche) in accordance with the manufacturer's instructions; the negative control slides were incubated with normal goat serum instead of the primary antibody. Normal control samples consisted of BMB specimens obtained for staging purposes, which were determined to be free of neoplasia and other abnormalities upon histological and immunohistochemical examinations.

Gomori stains were performed by means of automated staining system (BenchMark Special Stains; Ventana; Roche) using a specific kit (Reticulum II staining kit; Ventana; Roche) according with the manufacturer's instructions. Identification of

the reticulin fibers around BM vessels was used as an internal reaction control in each case.

Staining of EDA FN with IST-9 antibody on human BMBs was quantified by digital image procedures using ImageJ software. At least 10 or more digital color RGB (red, green, blue) images per stained BM sections from three HCs or patients at different phases of the disease were captured, converted to grayscale, thresholded, and analyzed with ImageJ to obtain the final staining measurement (expressed as percentage of total area). The same analysis has been performed on mouse BM sections to assess reticulin deposition and FN/type III collagen staining.

Cell culture and purification

For differentiation of mouse Mk's, BM cells were incubated with FITC Lineage cocktail antibodies and anti-FITC microbeads-conjugated antibodies according to the manufacturer's instructions (Miltenyi Biotech). Purified Lin^- populations were phenotypically defined to include 25–30% of c-Kit^+ LK cells and 3–4% of HSCs (LSK) as quantified by flow cytometry. Lin^- fractions were cultured for 4 d in DMEM (Gibco BRL) supplemented with 1% of penicillin/streptomycin, 1% of L-glutamine, and 10% of fetal bovine serum (Gibco BRL), in the presence of 10 ng/ml of murine recombinant TPO (Peprotech). In some experiments, Lin^- cells were also stimulated for 4 d with 1 µg/ml of EDA^+ and EDA^- recombinant peptides. To exclude potential contamination from TPO, EDA^- and EDA^+ peptides as well as plasma and cFNs were analyzed with an ELISA assay for human TPO (Human Thrombopoietin Quantikine ELISA kit; DTP00B; R&D Systems). However, we did not detect positive signals greater than the lower detection limit of this assay (31.3 pg/ml) from either reagent (5 µg/each for proteins, 1 µg/each for peptides).

For experiments of LSK cells proliferation, Lin^- cells were cultured in the presence of BrdU (10 µM) for 24 h and then analyzed by flow cytometry. MSCs were isolated from BM aspirates, expanded, and immunophenotypically characterized as previously described (Abbonante et al., 2016b; Avanzini et al., 2018). Cells were stimulated for 24 h with recombinant human TGF-β (10 ng/ml; Peprotech). All experiments were performed using early passage MSCs, maximum passage 5. Purification of BM cell fractions was performed as previously described (Malara et al., 2018). The whole BM was digested with collagenase IV (200 U/ml) at 37°C for 20 min and cell fractions purified with microbeads-conjugated anti-mouse CD45, Ter119, CD31, CD140a, or CD41-FITC and anti-FITC microbeads according to the manufacturer's instructions (Miltenyi Biotech).

Statistics

Values are expressed as mean ± SD. One-way ANOVA and two-way ANOVA followed by a Bonferroni post-test were used to analyze experiments. Mann–Whitney *U* test was used to analyze the difference in EDA FN levels in plasma samples between PMF and PV/ET and normal subjects. P values statistically significant were expressed as *, $P < 0.05$, **, $P < 0.01$, and ***, $P < 0.001$.

Online supplemental material

Fig. S1 shows the effects of TPO treatment on hematopoietic progenitors in mice with aberrant EDA splicing. Fig. S2 shows the effects of TLR4 inhibition on hematopoietic progenitors during BM fibrosis induction in wild-type mice. Fig. S3 shows the effects of TAK-242 treatment during BM fibrosis induction in mice with aberrant EDA splicing as well as in wild-type mice after the establishment of experimental fibrosis. Fig. S4 shows steady state thrombopoiesis and hematopoietic progenitors after experimental fibrosis in mice with TLR4 deletion. Fig. S5 shows specificity of ELISA for quantification of EDA FN in plasma samples.

Acknowledgments

We thank Amgen for providing romiplostim.

This paper was supported by the Italian Ministry of University and Research Future in Research (RBFR1299KO) to A. Malara; the Cariplo Foundation (2013-0717), Associazione Italiana per la Ricerca sul Cancro (AIRC IG 2016 18700), and the National Institutes of Health (R01-HL134829) to A. Balduini; Ricerca Finalizzata Giovani Ricercatori 2016 by the Italian Ministry of Health (GR-2016-02363136) to V. Abbonante and A. Malara; the National Institutes of Health (R35HL139926 and R01 NS109910) and the American Heart Association (18EIA33900009) to A.K. Chauhan; and Associazione Italiana per la Ricerca sul Cancro "Special Program Molecular Clinical Oncology 5x1000" to Associazione Italiana per la Ricerca sul Cancro–Gruppo Italiano Malattie Mieloproliferative to G. Barosi (project number 1005).

The funders had no role in study design, data collection and analysis, decision to publish, or preparation of the manuscript. The authors declare no competing financial interests.

Author contributions: A. Malara conceived the idea, designed and performed the experiments, analyzed the data, and wrote the manuscript. C. Gruppi and V. Abbonante performed the experiments and edited the manuscript. V. Rosti, M. Massa, and G. Barosi provided patient samples, analyzed the data, and edited the manuscript. D. Cattaneo, A. Iurlo, U. Gianelli, C.L. Balduini, and M.E. Tira analyzed the data and edited the manuscript. G. Barosi performed the statistical analysis on FN measurements in human plasma samples. L. De Marco, A.F. Muro, and A.K. Chauhan provided animals and reagents, analyzed the data, and edited the manuscript. A. Balduini supervised the project, conceived the idea, analyzed the data, and wrote the manuscript.

Submitted: 7 June 2018
Revised: 26 November 2018
Accepted: 9 January 2019

References

Abbonante, V., C.A. Di Buduo, C. Gruppi, A. Malara, U. Gianelli, G. Celesti, A. Anselmo, L. Laghi, M. Vercellino, L. Visai, et al. 2016a. Thrombopoietin/TGF-β1 Loop Regulates Megakaryocyte Extracellular Matrix Component Synthesis. *Stem Cells.* 34:1123–1133. https://doi.org/10.1002/stem.2285

Abbonante, V., C. Gruppi, P. Catarsi, M.A. Avanzini, M.E. Tira, G. Barosi, V. Rosti, and A. Balduini. 2016b. Altered fibronectin expression and

deposition by myeloproliferative neoplasm-derived mesenchymal stromal cells. *Br. J. Haematol.* 172:140–144. https://doi.org/10.1111/bjh.13471

Avanzini, M.A., V. Abbonante, P. Catarsi, I. Dambruoso, M. Mantelli, V. Poletto, E. Lenta, P. Guglielmelli, S. Croce, L. Cobianchi, et al.; AGIMM Investigators. 2018. The spleen of patients with myelofibrosis harbors defective mesenchymal stromal cells. *Am. J. Hematol.* 93:615–622. https://doi.org/10.1002/ajh.25047

Badalucco, S., C.A. Di Buduo, R. Campanelli, I. Pallotta, P. Catarsi, V. Rosti, D. L. Kaplan, G. Barosi, M. Massa, and A. Balduini. 2013. Involvement of TGFβ1 in autocrine regulation of proplatelet formation in healthy subjects and patients with primary myelofibrosis. *Haematologica.* 98: 514–517. https://doi.org/10.3324/haematol.2012.076752

Bhattacharyya, S., Z. Tamaki, W. Wang, M. Hinchcliff, P. Hoover, S. Getsios, E.S. White, and J. Varga. 2014. FibronectinEDA promotes chronic cutaneous fibrosis through Toll-like receptor signaling. *Sci. Transl. Med.* 6: 232ra50. https://doi.org/10.1126/scitranslmed.3008264

Borsi, L., P. Castellani, A.M. Risso, A. Leprini, and L. Zardi. 1990. Transforming growth factor-beta regulates the splicing pattern of fibronectin messenger RNA precursor. *FEBS Lett.* 261:175–178. https://doi.org/10.1016/0014-5793(90)80664-5

Ceglia, I., A.C. Dueck, F. Masiello, F. Martelli, W. He, G. Federici, E.F. Petricoin III, A. Zeuner, C. Iancu-Rubin, R. Weinberg, et al. 2016. Preclinical rationale for TGF-β inhibition as a therapeutic target for the treatment of myelofibrosis. *Exp. Hematol.* 44:1138–1155.e4. https://doi.org/10.1016/j.exphem.2016.08.007

Cervantes, F., B. Dupriez, A. Pereira, F. Passamonti, J.T. Reilly, E. Morra, A.M. Vannucchi, R.A. Mesa, J.L. Demory, G. Barosi, et al. 2009. New prognostic scoring system for primary myelofibrosis based on a study of the International Working Group for Myelofibrosis Research and Treatment. *Blood.* 113:2895–2901. https://doi.org/10.1182/blood-2008-07-170449

Chow, J.C., D.W. Young, D.T. Golenbock, W.J. Christ, and F. Gusovsky. 1999. Toll-like receptor-4 mediates lipopolysaccharide-induced signal transduction. *J. Biol. Chem.* 274:10689–10692. https://doi.org/10.1074/jbc.274.16.10689

Ciurea, S.O., D. Merchant, N. Mahmud, T. Ishii, Y. Zhao, W. Hu, E. Bruno, G. Barosi, M. Xu, and R. Hoffman. 2007. Pivotal contributions of megakaryocytes to the biology of idiopathic myelofibrosis. *Blood.* 110: 986–993. https://doi.org/10.1182/blood-2006-12-064626

Doddapattar, P., C. Gandhi, P. Prakash, N. Dhanesha, I.M. Grumbach, M.E. Dailey, S.R. Lentz, and A.K. Chauhan. 2015. Fibronectin Splicing Variants Containing Extra Domain A Promote Atherosclerosis in Mice Through Toll-Like Receptor 4. *Arterioscler. Thromb. Vasc. Biol.* 35: 2391–2400. https://doi.org/10.1161/ATVBAHA.115.306474

Dutta, A., R.E. Hutchison, and G. Mohi. 2017. Hmga2 promotes the development of myelofibrosis in Jak2^{V617F} knockin mice by enhancing TGF-β1 and Cxcl12 pathways. *Blood.* 130:920–932. https://doi.org/10.1182/blood-2016-12-757344

Fielding, C.A., G.W. Jones, R.M. McLoughlin, L. McLeod, V.J. Hammond, J. Uceda, A.S. Williams, M. Lambie, T.L. Foster, C.T. Liao, et al. 2014. Interleukin-6 signaling drives fibrosis in unresolved inflammation. *Immunity.* 40:40–50. https://doi.org/10.1016/j.immuni.2013.10.022

Han, F., J.R. Gilbert, G. Harrison, C.S. Adams, T. Freeman, Z. Tao, R. Zaka, H. Liang, C. Williams, R.S. Tuan, et al. 2007. Transforming growth factor-beta1 regulates fibronectin isoform expression and splicing factor SRp40 expression during ATDC5 chondrogenic maturation. *Exp. Cell Res.* 313:1518–1532. https://doi.org/10.1016/j.yexcr.2007.01.028

Hasselbalch, H.C. 2013. The role of cytokines in the initiation and progression of myelofibrosis. *Cytokine Growth Factor Rev.* 24:133–145. https://doi.org/10.1016/j.cytogfr.2013.01.004

James, C., V. Ugo, J.P. Le Couédic, J. Staerk, F. Delhommeau, C. Lacout, L. Garçon, H. Raslova, R. Berger, A. Bennaceur-Griscelli, et al. 2005. A unique clonal JAK2 mutation leading to constitutive signalling causes polycythaemia vera. *Nature.* 434:1144–1148. https://doi.org/10.1038/nature03546

Jarnagin, W.R., D.C. Rockey, V.E. Koteliansky, S.S. Wang, and D.M. Bissell. 1994. Expression of variant fibronectins in wound healing: cellular source and biological activity of the EIIIA segment in rat hepatic fibrogenesis. *J. Cell Biol.* 127:2037–2048. https://doi.org/10.1083/jcb.127.6.2037

Kaushansky, K. 2005. The molecular mechanisms that control thrombopoiesis. *J. Clin. Invest.* 115:3339–3347. https://doi.org/10.1172/JCI26674

Kelsh, R., R. You, C. Horzempa, M. Zheng, and P.J. McKeown-Longo. 2014. Regulation of the innate immune response by fibronectin: synergism between the III-1 and EDA domains. *PLoS One.* 9:e102974. https://doi.org/10.1371/journal.pone.0102974

Khan, M.M., C. Gandhi, N. Chauhan, J.W. Stevens, D.G. Motto, S.R. Lentz, and A.K. Chauhan. 2012. Alternatively-spliced extra domain A of fibronectin promotes acute inflammation and brain injury after cerebral ischemia in mice. *Stroke.* 43:1376–1382. https://doi.org/10.1161/STROKEAHA.111.635516

Kimura, A., T. Naka, T. Muta, O. Takeuchi, S. Akira, I. Kawase, and T. Kishimoto. 2005. Suppressor of cytokine signaling-1 selectively inhibits LPS-induced IL-6 production by regulating JAK-STAT. *Proc. Natl. Acad. Sci. USA.* 102:17089–17094. https://doi.org/10.1073/pnas.0508517102

Klampfl, T., H. Gisslinger, A.S. Harutyunyan, H. Nivarthi, E. Rumi, J.D. Milosevic, N.C. Them, T. Berg, B. Gisslinger, D. Pietra, et al. 2013. Somatic mutations of calreticulin in myeloproliferative neoplasms. *N. Engl. J. Med.* 369:2379–2390. https://doi.org/10.1056/NEJMoa1311347

Kohan, M., A.F. Muro, E.S. White, and N. Berkman. 2010. EDA-containing cellular fibronectin induces fibroblast differentiation through binding to alpha4beta7 integrin receptor and MAPK/Erk 1/2-dependent signaling. *FASEB J.* 24:4503–4512. https://doi.org/10.1096/fj.10-154435

Kohan, M., A.F. Muro, R. Bader, and N. Berkman. 2011. The extra domain A of fibronectin is essential for allergen-induced airway fibrosis and hyperresponsiveness in mice. *J. Allergy Clin. Immunol.* 127:439–446.e1-5. https://doi.org/10.1016/j.jaci.2010.10.021

Kuter, D.J., B. Bain, G. Mufti, A. Bagg, and R.P. Hasserjian. 2007. Bone marrow fibrosis: pathophysiology and clinical significance of increased bone marrow stromal fibres. *Br. J. Haematol.* 139:351–362. https://doi.org/10.1111/j.1365-2141.2007.06807.x

Kuter, D.J., G.J. Mufti, B.J. Bain, R.P. Hasserjian, W. Davis, and M. Rutstein. 2009. Evaluation of bone marrow reticulin formation in chronic immune thrombocytopenia patients treated with romiplostim. *Blood.* 114: 3748–3756. https://doi.org/10.1182/blood-2009-05-224766

Léon, C., K. Evert, F. Dombrowski, F. Pertuy, A. Eckly, P. Laeuffer, C. Gachet, and A. Greinacher. 2012. Romiplostim administration shows reduced megakaryocyte response-capacity and increased myelofibrosis in a mouse model of MYH9-RD. *Blood.* 119:3333–3341. https://doi.org/10.1182/blood-2011-08-373811

Liao, Y.F., P.J. Gotwals, V.E. Koteliansky, D. Sheppard, and L. Van De Water. 2002. The EIIIA segment of fibronectin is a ligand for integrins alpha 9beta 1 and alpha 4beta 1 providing a novel mechanism for regulating cell adhesion by alternative splicing. *J. Biol. Chem.* 277:14467–14474. https://doi.org/10.1074/jbc.M201100200

Losino, N., A. Waisman, C. Solari, C. Luzzani, D.F. Espinosa, A. Sassone, A.F. Muro, S. Miriuka, G. Sevlever, L. Barañao, and A. Guberman. 2013. EDA-containing fibronectin increases proliferation of embryonic stem cells. *PLoS One.* 8:e80681. https://doi.org/10.1371/journal.pone.0080681

Malara, A., C. Gruppi, P. Rebuzzini, L. Visai, C. Perotti, R. Moratti, C. Balduini, M.E. Tira, and A. Balduini. 2011. Megakaryocyte-matrix interaction within bone marrow: new roles for fibronectin and factor XIII-A. *Blood.* 117:2476–2483. https://doi.org/10.1182/blood-2010-06-288795

Malara, A., V. Abbonante, C.A. Di Buduo, L. Tozzi, M. Currao, and A. Balduini. 2015. The secret life of a megakaryocyte: emerging roles in bone marrow homeostasis control. *Cell. Mol. Life Sci.* 72:1517–1536. https://doi.org/10.1007/s00018-014-1813-y

Malara, A., C. Gruppi, G. Celesti, B. Romano, L. Laghi, L. De Marco, A.F. Muro, and A. Balduini. 2016. Brief Report: Alternative Splicing of Extra Domain A (EIIIA) of Fibronectin Plays a Tissue-Specific Role in Hematopoietic Homeostasis. *Stem Cells.* 34:2263–2268. https://doi.org/10.1002/stem.2381

Malara, A., C. Gruppi, G. Celesti, V. Abbonante, G. Viarengo, L. Laghi, L. De Marco, A.F. Muro, and A. Balduini. 2018. Alternatively spliced fibronectin extra domain A is required for hemangiogenic recovery upon bone marrow chemotherapy. *Haematologica.* 103:e42–e45. https://doi.org/10.3324/haematol.2017.173070

Mauviel, A., M. Daireaux, F. Rédini, P. Galera, G. Loyau, and J.P. Pujol. 1988. Tumor necrosis factor inhibits collagen and fibronectin synthesis in human dermal fibroblasts. *FEBS Lett.* 236:47–52. https://doi.org/10.1016/0014-5793(88)80283-7

Moretti, F.A., A.K. Chauhan, A. Iaconcig, F. Porro, F.E. Baralle, and A.F. Muro. 2007. A major fraction of fibronectin present in the extracellular matrix of tissues is plasma-derived. *J. Biol. Chem.* 282:28057–28062. https://doi.org/10.1074/jbc.M611315200

Mori, R., T. Kondo, T. Ohshima, Y. Ishida, and N. Mukaida. 2002. Accelerated wound healing in tumor necrosis factor receptor p55-deficient mice with reduced leukocyte infiltration. *FASEB J.* 16:963–974. https://doi.org/10.1096/fj.01-0776com

Muro, A.F., A.K. Chauhan, S. Gajovic, A. Iaconcig, F. Porro, G. Stanta, and F.E. Baralle. 2003. Regulated splicing of the fibronectin EDA exon is essential for proper skin wound healing and normal lifespan. *J. Cell Biol.* 162:149–160. https://doi.org/10.1083/jcb.200212079

Muro, A.F., F.A. Moretti, B.B. Moore, M. Yan, R.G. Atrasz, C.A. Wilke, K.R. Flaherty, F.J. Martinez, J.L. Tsui, D. Sheppard, et al. 2008. An essential role for fibronectin extra type III domain A in pulmonary fibrosis. *Am. J. Respir. Crit. Care Med.* 177:638–645. https://doi.org/10.1164/rccm.200708-1291OC

Nangalia, J., C.E. Massie, E.J. Baxter, F.L. Nice, G. Gundem, D.C. Wedge, E. Avezov, J. Li, K. Kollmann, D.G. Kent, et al. 2013. Somatic CALR mutations in myeloproliferative neoplasms with nonmutated JAK2. *N. Engl. J. Med.* 369:2391–2405. https://doi.org/10.1056/NEJMoa1312542

Norfolk, D.R., M. Bowen, B.E. Roberts, and J.A. Child. 1983. Plasma fibronectin in myeloproliferative disorders and chronic granulocytic leukaemia. *Br. J. Haematol.* 55:319–324. https://doi.org/10.1111/j.1365-2141.1983.tb01253.x

Okamura, Y., M. Watari, E.S. Jerud, D.W. Young, S.T. Ishizaka, J. Rose, J.C. Chow, and J.F. Strauss III. 2001. The extra domain A of fibronectin activates Toll-like receptor 4. *J. Biol. Chem.* 276:10229–10233. https://doi.org/10.1074/jbc.M100099200

Oyama, F., S. Hirohashi, Y. Shimosato, K. Titani, and K. Sekiguchi. 1990. Oncodevelopmental regulation of the alternative splicing of fibronectin pre-messenger RNA in human lung tissues. *Cancer Res.* 50:1075–1078.

Pardanani, A.D., R.L. Levine, T. Lasho, Y. Pikman, R.A. Mesa, M. Wadleigh, D. P. Steensma, M.A. Elliott, A.P. Wolanskyj, W.J. Hogan, et al. 2006. MPL515 mutations in myeloproliferative and other myeloid disorders: a study of 1182 patients. *Blood.* 108:3472–3476. https://doi.org/10.1182/blood-2006-04-018879

Schneider, R.K., S. Ziegler, I. Leisten, M.S. Ferreira, A. Schumacher, B. Rath, D. Fahrenkamp, G. Müller-Newen, M. Crysandt, S. Wilop, et al. 2014. Activated fibronectin-secretory phenotype of mesenchymal stromal cells in pre-fibrotic myeloproliferative neoplasms. *J. Hematol. Oncol.* 7: 92. https://doi.org/10.1186/s13045-014-0092-2

Shinde, A.V., C. Bystroff, C. Wang, M.G. Vogelezang, P.A. Vincent, R.O. Hynes, and L. Van De Water. 2008. Identification of the peptide sequences within the EIIIA (EDA) segment of fibronectin that mediate integrin alpha9beta1-dependent cellular activities. *J. Biol. Chem.* 283:2858–2870. https://doi.org/10.1074/jbc.M708306200

Speziale, P., L. Visai, S. Rindi, and A. Di Poto. 2008. Purification of human plasma fibronectin using immobilized gelatin and Arg affinity chromatography. *Nat. Protoc.* 3:525–533. https://doi.org/10.1038/nprot.2008.12

Tefferi, A., J. Thiele, A. Orazi, H.M. Kvasnicka, T. Barbui, C.A. Hanson, G. Barosi, S. Verstovsek, G. Birgegard, R. Mesa, et al. 2007. Proposals and rationale for revision of the World Health Organization diagnostic criteria for polycythemia vera, essential thrombocythemia, and primary myelofibrosis: recommendations from an ad hoc international expert panel. *Blood.* 110:1092–1097. https://doi.org/10.1182/blood-2007-04-083501

Tefferi, A., R. Vaidya, D. Caramazza, C. Finke, T. Lasho, and A. Pardanani. 2011. Circulating interleukin (IL)-8, IL-2R, IL-12, and IL-15 levels are independently prognostic in primary myelofibrosis: a comprehensive cytokine profiling study. *J. Clin. Oncol.* 29:1356–1363. https://doi.org/10.1200/JCO.2010.32.9490

Vannucchi, A.M., L. Bianchi, F. Paoletti, A. Pancrazzi, E. Torre, M. Nishikawa, M. Zingariello, A. Di Baldassarre, R.A. Rana, R. Lorenzini, et al. 2005. A pathobiologic pathway linking thrombopoietin, GATA-1, and TGF-beta1 in the development of myelofibrosis. *Blood.* 105:3493–3501. https://doi.org/10.1182/blood-2004-04-1320

Vannucchi, A.M., P. Guglielmelli, and A. Tefferi. 2009. Advances in understanding and management of myeloproliferative neoplasms. *CA Cancer J. Clin.* 59:171–191. https://doi.org/10.3322/caac.20009

Vardiman, J.W., J. Thiele, D.A. Arber, R.D. Brunning, M.J. Borowitz, A. Porwit, N.L. Harris, M.M. Le Beau, E. Hellström-Lindberg, A. Tefferi, and C.D. Bloomfield. 2009. The 2008 revision of the World Health Organization (WHO) classification of myeloid neoplasms and acute leukemia: rationale and important changes. *Blood.* 114:937–951. https://doi.org/10.1182/blood-2009-03-209262

Vellenga, E., J. Marrink, S. vd Geest, and E.G. de Vries. 1985. Plasma fibronectin in idiopathic myelofibrosis. *Br. J. Haematol.* 60:583–584. https://doi.org/10.1111/j.1365-2141.1985.tb07456.x

Villeval, J.L., K. Cohen-Solal, M. Tulliez, S. Giraudier, J. Guichard, S.A. Burstein, E.M. Cramer, W. Vainchenker, and F. Wendling. 1997. High thrombopoietin production by hematopoietic cells induces a fatal myeloproliferative syndrome in mice. *Blood.* 90:4369–4383.

Wang, D., K. Tao, J. Xion, S. Xu, Y. Jiang, Q. Chen, and S. He. 2016a. TAK-242 attenuates acute cigarette smoke-induced pulmonary inflammation in mouse via the TLR4/NF-κB signaling pathway. *Biochem. Biophys. Res. Commun.* 472:508–515. https://doi.org/10.1016/j.bbrc.2016.03.001

Wang, X.Q., H.Q. Wan, X.J. Wei, Y. Zhang, and P. Qu. 2016b. CLI-095 decreases atherosclerosis by modulating foam cell formation in apolipoprotein E-deficient mice. *Mol. Med. Rep.* 14:49–56. https://doi.org/10.3892/mmr.2016.5233

White, E.S., F.E. Baralle, and A.F. Muro. 2008. New insights into form and function of fibronectin splice variants. *J. Pathol.* 216:1–14. https://doi.org/10.1002/path.2388

Wu, D., J. Xie, X. Wang, B. Zou, Y. Yu, T. Jing, S. Zhang, and Q. Zhang. 2015. Micro-concentration Lipopolysaccharide as a Novel Stimulator of Megakaryocytopoiesis that Synergizes with IL-6 for Platelet Production. *Sci. Rep.* 5:13748. https://doi.org/10.1038/srep13748

Yanagida, M., Y. Ide, A. Imai, M. Toriyama, T. Aoki, K. Harada, H. Izumi, H. Uzumaki, M. Kusaka, and T. Tokiwa. 1997. The role of transforming growth factor-beta in PEG-rHuMGDF-induced reversible myelofibrosis in rats. *Br. J. Haematol.* 99:739–745. https://doi.org/10.1046/j.1365-2141.1997.4843288.x

Ylätupa, S., C. Haglund, P. Mertaniemi, E. Vahtera, and P. Partanen. 1995. Cellular fibronectin in serum and plasma: a potential new tumour marker? *Br. J. Cancer.* 71:578–582. https://doi.org/10.1038/bjc.1995.112

Zingariello, M., F. Martelli, F. Ciaffoni, F. Masiello, B. Ghinassi, E. D'Amore, M. Massa, G. Barosi, L. Sancillo, X. Li, et al. 2013. Characterization of the TGF-β1 signaling abnormalities in the Gata1low mouse model of myelofibrosis. *Blood.* 121:3345–3363. https://doi.org/10.1182/blood-2012-06-439661